Synthesis and Characterizations of Europium (Eu^{3+}) Ion- Doped Zinc Oxide Nanoparticles (ZnO-NPs) for Antibacterial and Photocatalytic Applications

Gemechu Barsisa Diriba

A Thesis Submitted to the Department of Applied Physics
School of Applied Natural Science

Presented in Partial Fulfillment of the Requirement for the Degree of Master's in Applied Physics

Office of Graduate Studies
Adama Science and Technology University

July, 2021

Adama, Ethiopia

Synthesis and Characterizations of Europium (Eu^{3+}) Ion- Doped Zinc Oxide Nanoparticles (ZnO-NPs) for Antibacterial and Photocatalytic Applications

Gemechu Barsisa Diriba

Advisor: Abebe Belay Gemta (Ph.D.)

A Thesis Submitted to the Department of Applied Physics
School of Applied Natural Science

Presented in Partial Fulfillment of the Requirement for the Degree of Master's in Applied Physics

Office of Graduate Studies
Adama Science and Technology University

July, 2021
Adama, Ethiopia

Declaration

I hereby declare that this Master thesis entitled **"Synthesis and Characterizations of Europium (Eu^{3+}) Ion- Doped Zinc Oxide Nanoparticles (ZnO-NPs) for Antibacterial and Photocatalytic Applications"** is my original work. That it, has not been submitted for the award of any academic degree, diploma or certificate in any other university. All sources of materials that are used for this thesis have been duly acknowledged through citation.

Name of the student	Signature	Date

Recommendation

I, the advisor of this Thesis, hereby certify that I have read the revised version of the thesis entitled **"Synthesis and Characterizations of Europium (Eu^{3+}) Ion- Doped Zinc Oxide Nanoparticles (ZnO-NPs) for Antibacterial and Photocatalytic Applications"** prepared under my guidance by **Gemechu Barsisa Diriba** submitted in partial fulfillment of the requirements for the degree of Master of Science in Applied Physics. Therefore, I recommend that the submission of the revised version of the thesis to the department following the applicable procedures.

Name of Advisor	Signature	Date

Approval Page

We, the advisors of the thesis entitled **"Synthesis and Characterizations of Europium (Eu^{3+}) Ion-Doped Zinc Oxide Nanoparticles (ZnO-NPs) for Antibacterial and Photocatalytic Applications"** and developed by **Gemechu Barsisa Diriba**, hereby certify that the recommendation and suggestions made by the board of examiners are appropriately incorporated into the final version of the thesis.

Major Advisor	Signature	Date

We, the undersigned, members of the Board of Examiners of the thesis by **Gemechu Barsisa Diriba** have read and evaluated the thesis entitled **"Synthesis and Characterizations of Europium (Eu^{3+}) Ion- Doped Zinc Oxide Nanoparticles (ZnO-NPs) for Antibacterial and Photocatalytic Applications"** and examined the candidate during the open defense. This is, therefore, to certify that the thesis is accepted for partial fulfillment of the requirement of the Degree of Masters of science in Applied Physics.

Chairperson	Signature	Date
Internal Examiner	Signature	Date
Eternal Examiner	Signature	Date

Finally, approval and acceptance of the thesis is contingent upon submission of its final copy to the Office of Postgraduate Studies (OPGS) through the Department Graduate Council (DGC) and School Graduate Committee (SGC).

_____	_____	_____
Department Head	Signature	Date
_____	_____	_____
School Dean	Signature	Date
_____	_____	_____
Office of Postgraduate Studies, Dean	Signature	Date

ACKNOWLEDGMENTS

First and foremost, I thank **"Almighty God"** for giving me the strength and faith in the successful completion of my thesis. And also I would like to thank him for blessing me with wonderful tutors, colleagues, and friends around me in these periods.

Next, I would like to express my most heartfelt and deepest gratitude to my thesis advisor Dr. Abebe Belay for his inspiring guidance, valuable discussions, continuous encouragement, moral support, constant motivation, constructive comments, and also his hard work and immense knowledge in the research area which helped me in the successful completion of this thesis work. The care he took fatherly approach is sincerely appreciable and is fortunate to have him as my thesis advisor and it is indeed a rare privilege to work under his guidance. His limitless guidance in my work is appreciable and invaluable. **I have been astonished to have such a Mentor**.

Secondly, it is a great pleasure to me to thanks Adama Science and Technology University for giving me this opportunity, facilities to complete my thesis work.

Thirdly, I would also like to thank the School of Applied Natural Science, Department of Applied Biology for allowing me to measure UV-Vis Spectroscopy and for testing my samples for Antibacterial Activity Applications, Department of Materials Science Engineering for allowing me to use XRD instruments to measure my samples and for testing my samples for photocatalytic Activities, and Addis Ababa University, College of Natural Science for allowing me to use FT-IR instruments.

Fourthly, my deepest gratitude goes to Efa Kebede Balcha and Kitesa Bekuma Gelato who did their most in keeping up me with morale and material supporting throughout the completion of this thesis work. They are polite, kind, and positive people.

Last but not the least, my fruitful indebtedness goes to my parents for their unreserved support. Above all the Lords, GOD, your names always praised. I love all of you!

TABLE OF CONTENTS

LIST OF TABLES

LIST OF FIGURES

LIST OF ABBREVIATIONS

BME……. Burstein-Moss Effect

CFU……Colony Forming Unit

DMSO……. ….Dimethyl Sulfoxide

DIW……Distilled Water

DLE……...Deep Level Emission

E.coli…….....Escherichia Coli

FDA…….. Food and Drug Administration

FT-IR…….Fourier Transform Infra-Red

MHA…… …M*ü*ller Hilton Agar

NPs……....Nanoparticles

NBE…… ….Near Band Edge

PL…….....Photoluminescence

PLD……Pulsed Laser Deposition

PVD……Physical Vapor Deposition

REE…….....Rare Erath Elements

ROS……Reactive Oxygen Species

S.aureus…….Staphylococcus aureus

UV-Vis……..Ultra Violet-Visible

XRD……..X-ray Diffraction

ZnO…….....Zinc Oxide

ZOI……Zones of Inhibition

ABSTRACT

In this research, Undoped and Europium (Eu^{3+}) ion-doped Zinc Oxide nanoparticles($Eu_{1-x}Zn_xO$)(x=0.03,0.06,0.09) were synthesized via the co-precipitation method using Zinc Nitrate Hexa-hydrate as the precursor material, Europium Nitrate pentahydrate as the dopant agent, and Sodium Hydroxide as the precipitating agent. The effects of varying the concentration of the Europium (Eu^{3+}) ion on the structure, optical properties method were investigated. The properties of Undoped and Europium (Eu^{3+}) ion-doped Zinc Oxide nanoparticles were characterized by XRD, UV-Vis, Photoluminescence spectroscopy, and FT-IR Spectroscopy. The XRD result showed that the Europium (Eu^{3+}) ion was successfully incorporated into the ZnO host matrix and the products were highly crystalline and have had significant quality. All synthesized samples were found to have a hexagonal wurtzite structure. UV-Vis absorption spectra revealed that, with increasing the amount of dopant concentration the values of energy band gap increases compared to the Undoped Zinc Oxide nanoparticles. Photoluminescence spectra confirmed that further doping of Europium (Eu^{3+}) ion predominantly enhances the visible emission with various series characteristics of blue and green emission compared to undoped ZnO which exhibits the near band emission. Fourier Transform Infra-Red (FT-IR) spectral analysis indicated the presence of functional groups such as, C=O, C-H, C=H, O-H, and ZnO NPs attached to the undoped and Europium (Eu^{3+}) ion doped Zinc Oxide nanoparticles. The antibacterial activity of undoped and Europium (Eu^{3+}) ion doped Zinc Oxide nanoparticles were also investigated. The result confirmed that Gram –ve bacteria were found to have a great potential than Gram +ve bacteria. The photocatalytic activity of Europium (Eu^{3+}) ion doped Zinc Oxide nanoparticles has higher performance than Undoped Zinc Oxide nanoparticles.

Keywords: *Zinc Oxide Nanoparticles, Nanoparticles, Co-precipitation method, Anti-bacterial activity, photocatalytic activity, Photoluminescence.*

1. INTRODUCTION

1.1.Background of the Study

In recent years, industrial pollutants found in the environment particularly air and water poses serious health hazards to human life. Therefore, the developments of a cost-effective method to control water pollution consider a top priority in current research (Ramírez et al., 2021). The development of the economy and the popularization of industrialization, the rapid improvement of human living standards have exposed serious environmental pollution problems, exposing a serious threat to human health and hindering the sustainable development of society. A lot of researchers have made great efforts to explore more catalysts or novel materials to degrade organic and toxic pollutants of wastewater. Fortunately, energy shortage and water pollution problems can be partially solved by semiconductor photo-catalysis technology, which has been the research focus recently (Guan et al., 2019). The semiconducting materials have been used in the photo-catalysis field (Guan et al., 2019). It is widely used in the photocatalytic degradation of organic dyes and photocatalytic decomposition of generating hydrogen from water.

Semiconducting nanoparticles have attracted wide attention in this area due to their unique structural and functional properties which are utilized for potential applications in energy and environmental nanotechnology. Semiconductors are widely used as a photo- catalyst to convert harmful toxic organic pollutants into harmless elements. Hence, it is used to eliminate environmental pollutants and attracted researchers to work on the area with a great deal of interest in the recent past (Srinivasan, 2019). Among the vast majority of semiconductor photo- catalysts, rare earth elements (REE) doped Zinc Oxide nanoparticles (ZnO-NPs) are the prominent strategy to improve the properties of photocatalytic efficiency.

Hence, the photo-catalytic activity of ZnO has to be enhanced than the other materials by employing various strategies. One of the important strategies in improving the photo-catalytic properties is doping the metal oxides which eventually results in the variation of surface area and the incorporation of dopant ions generates lattice defects and modify bandgap energy and its visible light response (Srinivasan,

2019). Much rare-earth-doped ZnO photo- catalyst was used such as Ce^{3+}, Dy^{3+}, La^{3+}, and Nd^{3+} for the photo degradation of organic pollutants.

Recently, great progress in the development of nanoscience and nanotechnology has allowed us to create new nano-sized materials having unique electronic and optical properties quite different from those of their bulk counterpart state. These size-dependent properties of nanomaterials have been studied and utilized in various electronic and optical devices. Simultaneously, intensive research efforts have been made to understand and control the collective properties of nanoparticles (Choi et al., 2007). In recent years, many researchers have been waxed and waned in semiconductor materials due to their prominent properties. These unique properties are fundamental to research application, due to their unique size and shape-dependent optical, electrical, magnetic, photocatalytic, biomedical properties (Bomila et al., 2018).

Metal oxide nanoparticles have been the subject of extensive interest due to their potential credence in a wide range of activities. Among different metal oxide nanoparticles, Zinc oxide nanoparticles (ZnO-NPs) are paramount n-type inorganic semiconductor material with a wide direct bandgap of 3.37 eV and high exciton binding energy 60meV (Kaur et al., 2018). Zinc oxide nanoparticles (ZnO-NPs) possess several interesting properties such as optical transparency, electric conductivity, piezoelectricity, non-toxicity, wide availability, low cost, and stability (Tafreshi, 2020). Additionally, Zinc Oxide nanoparticles (ZnO-NPs) are materials with multifunctional and salient properties such as high photostability, low dielectric constant, high chemical stability, high electrochemical coupling coefficient, and a broad range of radiation absorption (Karakız et al., 2008).

Owing to its unique and versatile properties, zinc oxide nanoparticles (ZnO-NPs) have been utilized as an essential candidate for multifunctional applications such as optoelectronics (Karakız et al., 2008), solar cells (Kaur et al., 2018), laser technology (Preethi et al., 2016), light-emitting diodes (LEDs) (Dumrongrojthanath & Phuruangrat, 2021), surface acoustic wave's device (Karthick, 2018), antimicrobial and antifungal activity (R. K. Sharma & Ghose, 2015), luminescent, and gas sensor devices (Vijayaprasath et al., 2015) Moreover, it exhibits better performance in degrading of various environmental pollutants: pesticides, detergents, dyes, and

volatile organic compounds by transforming into carbon dioxide, water, and mineral acids under ultraviolet-visible (UV) light irradiation (Phuruangrat et al., 2016). Because of its hardness, rigidity, and piezoelectric constant, it is an important material in the ceramics industry, while its low toxicity, biocompatibility, and biodegradability make it a material of interest for biomedicine and in pro-ecological systems (Rl et al., 2019). ZnO-NPs have been synthesized using different methods in various morphologies such as fibers, wires, flowers, rods, mallets, tetrapods, and rings with glitter properties (R. K. Sharma & Ghose, 2015).

Due to the diverse applications of these nanoparticles, zinc oxide nanoparticles (ZnO-NPs) have been devoted by several synthesis methods. These techniques includes for instance, hydrothermal method (Vijayaprasath et al., 2015), co-precipitation (Ntwaeaborwa et al., 2017), pulsed laser deposition (PLD) (Kaur et al., 2018), sol-gel method (Azri et al., 2012), microwave-assisted combustion, and solid-state reaction (Xin, 2018). Among the above techniques, a co-precipitation is a promising option for the synthesis and large-scale production of ZnO nanoparticles (Karthick, 2018). On the one hand, this technique is a promising technique that is non-expensive, easy to manipulate, effective, easy to control mixing rate, easy to adjust dopant concentration.

Many researchers have attempted doping methods of zinc oxide nanoparticles (ZnO-NPs) to improve their prominent properties. A few years ago, several researchers have been focused on semiconducting materials doped with rare earth elements (REE) ions. (Karthick, 2018), synthesized lanthanum (La^{3+}) ion-doped with Zinc Oxide nanoparticles (ZnO-NPs) with the co-precipitation method. They investigated the effects of lanthanum doping concentration on the structures, morphologies, and photoluminescence properties. Using wet chemical co-precipitation, (Badreddine et al., 2018) Synthesized and researched the influence of the effect of samarium doping on the structural, morphological, optical, and magnetic properties of ZnO nanoparticles using different characterization techniques. Semiconductor materials doped with rare-earth (REE) are technologically significant materials. One of the most fundamental and efficient ways to alter the properties of semiconducting material is through the doping method. For semiconducting material, the doping method has been extensively utilized to tailor the optical, structural, and morphological properties. On the other side, Doping means intentionally introducing

impurities into an extremely pure semiconductor. It is well known that the doping of impurities greatly affects the basic physical properties, (e.g., electrical, optical, and morphological properties) (Universit & Ilmenau, 2017). A large number of studies and investigations on doping of rare earth elements (REE) ions into the ZnO matrix led to tuning the optical, structural, and morphological properties of the material. In extant studies, rare earth elements (REE) ions- doped with Zinc Oxide nanoparticles (ZnO-NPs) has been used to improve the properties and they are exhaustively used in optoelectronic devices to vary the properties of the materials. Rare earth elements (REE) such as (Eu^{3+}, Tb^{3+}, Er^{3+}, Dy^{3+}, Sm^{3+}, Gd^{3+}, and La^{3+}) ions generally have high luminescent intensity because their 4f intra shell transitions can generate narrow and intense emission lines (Ma & Wang, 2012). Among the rare earth elements (REE), Europium (Eu^{3+}) ion has been the topic of interest in this study.

Furthermore, Europium (Eu^{3+}) ion-doped has many applications for instance easy incorporation into host ZnO-NPs because of its larger radius of Europium (Eu^{3+}) ion (0.094 nm) with that of Zinc (Zn^{2+}) ion (0.074 nm) which in turn enhances their application.

Antimicrobial activities of metal oxide (ZnO, MgO, and CaO) nanoparticles against *Staphylococcus aureus*, and *Escherichia coli* were quantitatively evaluated in culture media. It is considered that the detected active oxygen species generated by these metal oxide particles could be the main mechanism of their antibacterial activity (Gunalan et al., 2013). Antibacterial activity of zinc oxide nanoparticles (ZnO-NPs) has received significant interest worldwide particularly by the implementation of nanotechnology to synthesize particles in the nanometer regime. ZnO-NPs exhibit attractive antibacterial properties due to increased specific surface area as the reduced particle size leading to enhanced particle surface reactivity. Particular emphasis was given to bactericidal and bacteriostatic mechanisms with a focus on the generation of reactive oxygen species (ROS) including hydrogen peroxide (H_2O_2), OH^- (hydroxyl radicals), and O_2^{-2} (peroxide). ROS has been a major factor for several mechanisms including cell wall damage due to ZnO-localized interaction, enhanced membrane permeability, internalization of NPs due to loss of proton motive force, and uptake of toxic dissolved zinc ions. These have led to mitochondria weakness, intracellular outflow, and release in gene expression of oxidative stress which caused eventual cell growth inhibition and cell death. In some cases, enhanced antibacterial activity can be

attributed to surface defects on ZnO abrasive surface texture (Sirelkhatim et al., 2015).

The antibacterial activity of zinc oxide nanoparticles (ZnO-NPs) has been extensively studied and investigated. Among the bacterial strains, gram-positive bacteria (*Staphylococcus aureus (S. aureus))* (ATCC-25923) and gram-negative bacteria (*Escherichia coli, (E.coli*)) (ATCC-25922) were used as test microorganisms in this study. This study is the first report on the work of Eurpium (Eu^{3+}) ion-doped Zinc Oxide nanoparticles (ZnO-NPs) synthesized by chemical route technique for nanomedicinal applications. To the best of the author's knowledge, gram-positive bacteria have more resistivity than gram-negative bacteria due to their polarity difference of cell membrane and intracellular antioxidant content. In our study, as the concentration of dopant amount increases the antibacterial possessed higher activity as compared to the Undoped Zinc Oxide nanoparticles (ZnO-NPs).

To date, many scholars have been involved in the synthesis and characterization of Europium (Eu^{3+}) ion-doped by Zinc Oxide nanoparticles (ZnO-NPs) in different conditions for different applications at different precursor elements by using several synthetic routes. In the present work, the synthesis and characterization of Europium (Eu^{3+}) ion-doped by Zinc Oxide nanoparticles (ZnO-NPs) have been extensively used for antibacterial and photocatalytic activity applications.

Therefore, the general objective of this paper is to synthesize and characterize Europium (Eu^{3+}) ion-doped Zinc Oxide nanoparticles (ZnO-NPs) for antibacterial and photo-catalytic applications. And the specific objectives of this paper are to 1. Synthesize Europium (Eu^{3+}) ion-doped Zinc Oxide nanoparticles (ZnO-NPs), 2. Characterize Europium (Eu^{3+}) ion-doped Zinc Oxide nanoparticles (ZnO-NPs) using various spectroscopic techniques such as X-Ray Diffractometer (XRD), UV-Vis Spectroscopy, Fourier Transformation Infra-Red (FTIR) Spectroscopy, and Photoluminescence (PL) Spectroscopy, 3. Analyze the effect of doping of the Europium (Eu^{3+})- ion into Zinc Oxide nanoparticles (ZnO-NPs), 4. Apply Europium (Eu^{3+}) ion-doped Zinc Oxide nanoparticles (ZnO-NPs) on the antibacterial activities, and 5. Apply Europium (Eu^{3+}) ion-doped Zinc Oxide nanoparticles (ZnO-NPs) for the photo-catalytic activities.

1.2.Thesis Organization

This thesis has been composed of five chapters, organized as follows, each chapter focusing on a particular aspect. Starting with the general introduction, in chapter one, an overview of the study, synthesis methods, general and specific objectives of the study, and the glitter properties of rare earth elements (REE) have been presented. This elaborates the state-of-the-art from the recent research status on the effect of doping rare earth elements (REE) by Zinc Oxide nanoparticles (ZnO-NPs), and it highlights the visible outcome of the study carried out, which serves as a good platform for future perspectives followed by the research objectives were introduced.

Chapter two has been devoted to the background of the study, basic properties of Zinc Oxide nanoparticles (ZnO-NPs), fabrication of rare earth elements (REE) by Zinc Oxide nanoparticles (ZnO-NPs), characterization techniques of Zinc Oxide nanoparticles (ZnO-NPs), application of Zinc Oxide nanoparticles (ZnO-NPs), and antibacterial applications Zinc Oxide nanoparticles (ZnO-NPs) were also briefly discussed in detail.

In chapter three, the materials and methods of the study were presented. In this subsection, the chemicals, solvents, and instruments used to carry out this work were described. In the latter sections, the experimental procedures developed to synthesize and characterize Europium (Eu^{3+}) ion-doped by Zinc Oxide nanoparticles (ZnO-NPs) and determination of antibacterial test of Europium (Eu^{3+}) ion-doped by Zinc Oxide nanoparticles (ZnO-NPs) have been reported.

In chapter four, the effects of Europium (Eu^{3+}) ion-doped by Zinc Oxide nanoparticles (ZnO-NPs) on optical, structural, emission intensity in respective to the host Zinc Oxide nanoparticles (ZnO-NPs) were predicted. Additionally, the effects of doping applied on the antibacterial and photo-catalytic activity of Europium (Eu^{3+}) ion-doped by Zinc Oxide nanoparticles (ZnO-NPs) were also presented.

Finally, in chapter five, conclusions and recommendations for future works have been provided.

2. REVIEW OF THE LITERATURE

In this chapter, the concepts of nanoparticles, nanotechnology, nanoscience, were reviewed in the literature broadly. Additionally, the basic properties related to Zinc Oxide nanoparticles (ZnO-NPs), synthesis routes, characterization techniques, application of Zinc Oxide nanoparticles (ZnO-NPs), antibacterial activity were discussed.

2.1.Nanoparticles

Nanoparticles (NPs) are known as controlled or manipulated particles at the atomic level (1–100 nm) (Sirelkhatim et al., 2015). Nanoparticles are is a special group of materials with unique features and extensive applications in diverse fields. Studying these particular features has always been of great interest to many scientists. Nanoparticles display unique properties in comparison with their bulk size counterparts. A large number of materials that were considered to be safe develop toxicity at nano-size ranges which are mainly related to the increased specific surface area and high reactivity of nano-sized materials (Emami-karvani & Chehrazi, 2011).

2.2.Nanoscience and nanotechnology

Nanotechnology is the art and science of manipulating matter at the nanoscale to create new and unique materials and products with enormous potential to change society (Upadhyaya et al., 2018). This technology is capable of providing miscellaneous novel applications that range from innovative fabric compounds, food processing, and agricultural production to sophisticated medicinal techniques. It is considered as the synthesis, characterization, and exploration of materials in the nanometer region (1–100 nm) (Sirelkhatim et al., 2015). Likewise, Nanotechnology is a scientific and engineering technology conducted at the Nano-scale, such as in the fields of compound fabric manufacturing, food processing, agricultural processing, and engineering, as well as in medical and medicinal applications (Hoseinzadeh et al., 2017).

Another possible definition is the study of phenomena and manipulation of materials at atomic, molecular, and macromolecular scales, where properties differ from the bulk counterpart scales. In other words, it is a horizontal integrating

interdisciplinary science that cuts across all vertical sciences and engineering disciplines.

Nanotechnology is the manipulation or self-assembly of individual atoms, molecules, or molecular clusters into structures to create materials devices with new or vastly different properties (Rl et al., 2019). Nanotechnology can be understood as a technology of design, fabrication, and applications of nanostructures and nanomaterials, as well as a fundamental understanding of the physical properties and phenomena of nanomaterials and nanostructures (Ahmed et al., 2015).

2.3.Fundamental properties of Zinc Oxide nanoparticles (ZnO-NPs)

ZnO is an inorganic compound that occurs naturally as a mineral zincite or is chemically synthesized. It is an n-type semiconductor with a direct bandgap of 3.37 eV (368 nm) and large exciton binding energy at room temperature of 60 meV is one of the most common materials because it has outstanding physical and chemical stability, low cost, high oxidizing power, high exciton binding energy, high transparency, high thermal stability, high biocompatibility. It has been widely used for optical, electrical, optoelectronic, catalytic, and photochemical properties, including optical waveguides and transparent conducting coatings. which makes it a suitable material for colossal applications such as flat panel displays (Sa-nguanprang et al., 2019) (Phuruangrat et al., 2014).

2.3.1. Crystal structure of Zinc Oxide nanoparticles (ZnO-NPs)

At room temperature and ambient pressure, Zinc Oxide nanoparticles (ZnO-NPs) have three different structures, namely the hexagonal wurtzite, zinc blende, and rock salt structures. Among, the most common structure of Zinc Oxide nanoparticles (ZnO-NPs) is the wurtzite crystal structure. The crystalline ZnO has a wurtzite structure that has a hexagonal unit cell with two lattice parameters of ‘a’ and ‘c’ and belongs to the space group of C^4_{6v} or P63mc. The lattice parameters of the hexagonal unit cells mostly range from 0.32475 to 0.32501 nm for ‘a’ and from 0.52042 to 0.52075 nm for ‘c’. The structure of ZnO can be simply described as several alternating planes composed of tetrahedrally coordinated O^{2-} and Zn^{2+} ions, stacked alternately along the c-axis. . In the wurtzite structure, each zinc ion is surrounded by four oxygen ions which are arranged in tetrahedral coordination, and alternatively each oxygen ion is surrounded by four zinc ions that are tetrahedrally coordinated

along the c-axis. The tetrahedral arrangement of the zinc and oxygen ions gives rise to a non-centrosymmetric crystal structure of ZnO, consisting of two sub-lattices of zinc and oxygen atoms penetrating each other to form a hexagonal close-packed structure. When the bonds along the c-direction are from cation (Zn) to anion (O) the polarity is referred to be as Zn polarity.

In addition to polar surfaces, it also has non-polar surfaces. The four most common faces of wurtzite ZnO are the polar Zn-terminated (0001) and O-terminated ($000\bar{1}$) faces (c-axis oriented), and the ($2\bar{1}\bar{1}0$) (a-axis) and ($01\bar{1}0$) faces that contain an equal number of Zn and O atoms. The ($2\bar{1}\bar{1}0$) (a-axis) and ($01\bar{1}0$) faces are non-polar surfaces and have lower energy than the {0001} facets. Furthermore, the polar surfaces and the ($01\bar{1}0$) surfaces are found to be stable; however, the ($2\bar{1}\bar{1}0$) face is less stable and generally has a higher level of surface roughness than its counterparts. It has been observed that the origination of various shapes of the ZnO crystals is due to the relative growth rates of different crystal facets and differences in the growth rates of different crystal planes (Hahn, 2011) (Wang, 2004)(Stefaniuk et al., 2018).

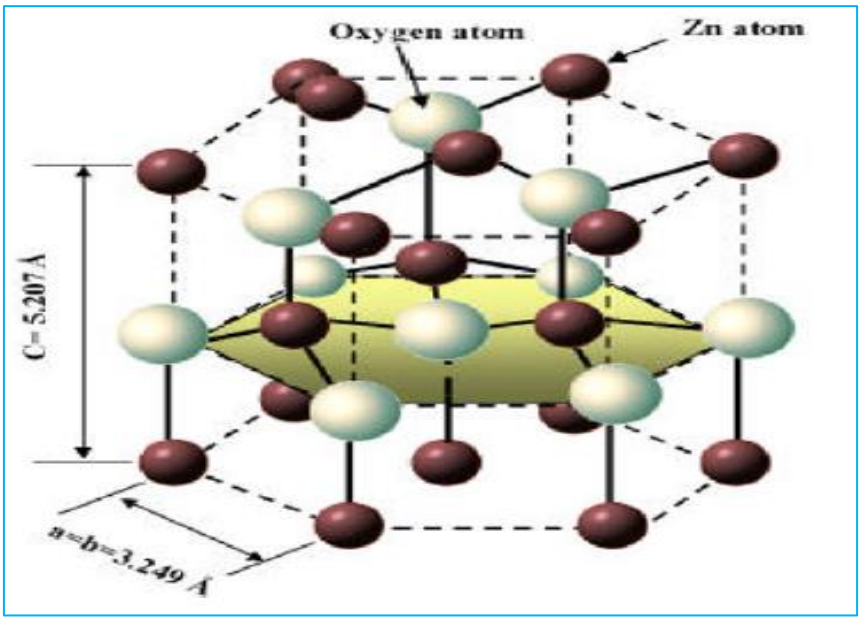

Figure 2.1: The hexagonal wurtzite structure model of ZnO. The tetrahedral coordination of Zn-O is shown. O atoms are shown as larger white spheres while the Zn atoms are smaller brown spheres (Hahn, 2011).

The crystal structures were investigated by XRD (x-ray diffraction) which is based on Wulf-Bragg's law presented in Eq (2.1).

According to Bragg's law (Gadalla et al., 2018),

$$n\lambda = 2d\sin\theta \tag{2.1}$$

Where n is the order of diffraction (usually n = 1), λ is the X-ray wavelength and d is the spacing between planes of given Miller indices h, k, and l.

The plane spacing d to the lattice parameters ('a' and 'c') for the wurtzite hexagonal structure of ZnO can be calculated from (Karthikeyan et al., 2019).

$$\frac{1}{d^2{}_{hkl}} = \frac{4}{3}\left(\frac{h^2 + hk + k^2}{a^2} + \frac{l^2}{c^2}\right) \tag{2.2}$$

with the first order approximation (n = 1) Eq (2.2) above can be re written as Eq (2.3)(Devi & Velu, 2016b).

$$\sin^2\theta = \frac{\lambda^2}{4}\left(\frac{4}{3}\left(\frac{h^2 + hk + k^2}{a^2}\right) + \frac{l^2}{c^2}\right) \tag{2.3}$$

In the case of the wurtzite phase, the lattice parameters are calculated by using the formula Eqs (2.4-2.5) (Raj et al., 2017).

$$a = \frac{\lambda}{\sqrt{3}\sin\theta_{100}} \tag{2.4}$$

$$c = \frac{\lambda}{\sin\theta_{002}} \tag{2.5}$$

Another method to authenticate the presence of dopant concentration is to estimate the presence of the bond length (L). The bond lengths are calculated using the relation of Eq(2.6) (Vijayaprasath et al., 2016).

$$L = \sqrt{\left(\frac{a^2}{3} + \left(\frac{1}{2} - u\right)^2 c^2\right)} \tag{2.6}$$

The positional parameter in the wurtzite structure and is determined by the amount by which each atom gets displaced for the 'c' axis given by Eq (2.7) (Raj et al., 2016).

$$u = \frac{a^2}{3c^2} + \frac{1}{4} \tag{2.7}$$

The average crystallite sizes of the synthesized samples were calculated from XRD spectra using Debye-Scherrer's equation Eq (2.8)(Badreddine et al., 2018).

$$D = \frac{K\lambda}{\beta_{hkl} \cos\theta} \tag{2.8}$$

Where D is the average crystallite size of the particle, λ is the incident X-ray wavelength, β is the angular peak width at half maximum in radians, and θ is Bragg's diffraction angle.

The dislocation density, δ is a measure of the number of defects and vacancies in the crystal, which can be determined from the crystallite size (D) using the relation in Eq (2.9) (Badreddine et al., 2018).

$$\delta = \frac{1}{D^2} \tag{2.9}$$

The lattice expansion is quantified by the measurement of micro-strain which is given by Eq (2.10) (Choudhary, 2020).

$$\varepsilon = \frac{\beta \cos\theta}{4} \tag{2.10}$$

The unit cell volumes (V) for the hexagonal system were found from Eq (2.11) (Karthikeyan et al., 2019).

$$V = \frac{\sqrt{3}a^2 c}{2} = 0.866 a^2 c \tag{2.11}$$

Atomic packing fraction has been calculated using the formula Eq (2.12) (Kumar et al., 2016).

$$APF = \frac{2\pi a}{3\sqrt{3}c} \tag{2.12}$$

2.3.2. Physical properties and parameters of Zinc Oxide nanoparticles (ZnO-NPs)

Nanotechnology applications are greatly depending on the fundamental properties of the nanomaterial. Therefore, knowing the fundamental physical properties of ZnO is crucial to the rational design of functional devices. It should be noted that as the dimension of the semiconductor materials shrinks down to nanometer scale, some of

their physical properties change due to "quantum size effects". The physical parameters of the hexagonal wurtzite ZnO are summarized in Table 2.1.

Table 2.1: The basic physical properties of Zinc Oxide nanoparticles (ZnO-NPs) in wurtzite structure (Lu et al., 2005).

Property		Value
Lattice constants at (300K)	a	0.324 95 nm
	c	0.520 69 nm
	$\frac{c}{a}$	1.602 (ideal hexagonal structure shows 1.633)
	u	0.345
Density		5.606 gcm^{-3}
Stable phase at 300 K		Wurtzite
Melting point		1975 ℃
Linear expansion coefficient (/℃)		a: 6.5×10^{-6} c: 3.0×10^{-6}
Static dielectric constant		8.656
Refractive index		2.008, 2.029
Energy gap (300 K)		3.4 eV (direct band gap)
Exciton binding energy		60.0 meV
Magnetic susceptibility(χ)		$-27.2x10^{-6}\ cm^3mole^{-1}$
Electron effective mass		0.24
Hole effective mass		0.59
Bulk hardness, H (GPa)		5.0 ± 0.1
Electron mobility (T = 300 K) for low n-type conductivity		200 $cm^2V^{-1}s^{-1}$

Hole mobility (T = 300 K) for low n-type conductivity	5-50 $cm^2V^{-1}s^{-1}$

2.3.3. Optical properties of Zinc Oxide nanoparticles (ZnO-NPs)

The photoluminescent property of Zinc Oxide nanoparticles (ZnO-NPs) excited by UV radiation is usually exhibited by two prominent broad bands. The first band is located at 380nm in the Ultra Violet emission and is related to the band to band transition, known as near band edge emission (NBE) (Vijayaprasath et al., 2018), the second band is located in the visible region (450-800nm) and it is attributed to the deep-level emission (DLE). . It is well known that the visible emission of ZnO is due to the radiative recombination of a photogenerated hole with an electron occupying the oxygen vacancy. The well-known defects in ZnO are oxygen vacancies (V_o), oxygen interstitials (O_i), oxygen antisites (Zn_O), zinc vacancies (V_{zn}), zinc interstitials (Zn_i) and zinc antisites (O_{Zn}). Visible light emission is a result of electron-hole recombination taking place at defect states (Ntwaeaborwa et al., 2017).

(D. K. Sharma et al., 2016) reviewed that, the PL spectra of Zinc Oxide nanoparticles (ZnO-NPs) doped with Cerium (Ce^{3+}) ions contain two strong emission peaks at UV (388.4 nm) and visible range (535 nm). The UV emission is due to the near band–edge (NBE) emission of ZnO, which generates from the recombination of exciton-exciton through collision process. The emission in the visible range is referred to as a green emission, which is the emission outcome from the radiative recombination of a photo-generated hole with an electron occupying the oxygen vacancy. This green emission is due to the defects i.e. oxygen vacancy, zinc vacancy, oxygen interstitial, zinc interstitial.

2.4.Characteristics of Europium (Eu^{3+}) ion and Need for Doping

For using ZnO NPs in advanced and sophisticated industrial applications, numerous studies are taking place to find the optimum solution for enhancing the for providing wide bandgap semiconductors continues to performance properties of ZnO without changing its physiochemical properties. Thus, modifications are taking for improving its performance properties (Daksh & Agrawal, 2016). It has been extensively proven that modifications of ZnO nanoparticles with rare earth elements (REE) could improve their properties. These elements are widely exploited for the doping of ZnO

nanomaterials and to properly modify the corresponding electronic band structure. The change in the bandgap and the generation of trap states make Rare Earth doping interesting and from the luminescence point-of-view, this increases the possibility of ZnO being used as the imaging agent.

2.5.Novel Routes of synthesizing Zinc Oxide nanoparticles (ZnO-NPs)

The synthesis of nanomaterials and nanostructures is an important aspect of nanoscience and nanotechnology. New physical properties and applications of nanomaterials are only possible when nanostructured materials are made available with desired size, shape, morphology, crystal structure, and chemical composition. There are two general approaches for the synthesis of nanomaterials. Nanostructures, nanomaterials, and nanocomposites can be fabricated using two different techniques, top-down and bottom-up methods.

2.5.1. Top-down method

The top-down method is a physical method in which a microcrystalline or bulk material has been broken down again and again into small pieces with various lithographic techniques like grinding, milling, etc. The microcrystalline or bulk material becomes like a powder, which is in the form of nanomaterials. All the solid-state routes fall into this category including, mechanical attrition.

2.5.2. Bottom-up method

The bottom-up method is a chemical method where nanomaterials are building up from the bottom to upwards. This means that adding (self-assembling) very small atoms or molecules up to the required size. All techniques that start with liquid and gas as the starting material fall into this category including, physical vapor deposition (PVD), chemical vapor deposition, spray conversion processing, sol-gel process, wet chemical method, self-assembly, and green synthesis method. It also provides rigorous control of the size and shape of the nanoparticles.

2.6.Methods for synthesizing Europium (Eu^{3+}) ion- doped with Zinc Oxide nanoparticles (ZnO-NPs)

In the last decades, several sophisticated approaches have so far been used to synthesize rare earth elements (REE) doped by Zinc Oxide nanoparticles (ZnO-NPs) which in turn utilized in many fields for different glitter applications widely. In doing so, there are different methods used to synthesize rare earth elements (REE) doped by Zinc Oxide nanoparticles (ZnO-NPs) sol-gel method (Ghrib et al., 2021), chemical

precipitation, hydrothermal reaction (Gadalla et al., 2018), the hydrothermal method (Pradeev et al., 2018).

2.6.1. Co-precipitation method

Co-precipitation takes place when any solution is supersaturated to form precipitates with another substance. In this method, an inorganic metal salt is dissolved in the solvent and these formed species are hydrolyzed by adding a basic solution example NaOH or KOH. By the action of the cationic solution, solutions are condensed with each other to form a metal hydroxide precipitate. The formed precipitate has undergone several processes, such as filtration, annealing, and drying, to collect nanopowders of crystalline metal oxides. The main advantage of using this method is that it is very economical and metal oxide nanopowders can easily be synthesized. The co-precipitation process can be affected by several parameters such as pH, temperature, the concentration of the solutes, annealing, and effect of catalyst, reaction time, and drying for obtaining metal oxides nanostructures of different morphologies. Additionally, these synthetic routes have been popularly adopted to synthesize by using ZnO NPs due to their low cost and high yield of nanoparticles with uniform size (Devi & Velu, 2016a).

2.6.2. Sol-gel process

The sol-gel method is defined as a wet chemical route for the synthesis of colloidal dispersions (sols) of inorganic and organic-inorganic hybrid materials, particularly oxides and oxides-based hybrid at relatively low temperatures. This process involves a formation of an inorganic network of colloidal suspension sol followed by gelation of the sol solution to form a continuous liquid phase gel. Thus formed gel can be used to fabricate various nanomaterials and nanostructures such as powders, aerogels, xerogels, etc. Several precursors can serve as sol forming constitutes such as metal alkoxides, metal-organic compounds, salts of inorganic acids, salts of organic acids, etc. However, the most commonly used precursors are metal alkoxides; compounds in which a metal is bonded to one or more alkyl groups through an intermediate oxygen atom. The addition of an acid or base catalyst is also common in sol-gel processes to increase the rate of the reaction.

This method can be used for fabrication purposes, mainly of metal oxides, such as silicon. In this process, the monomers are converted into colloidal solutions acting as precursors for the gel formation using discrete particles. The precursors that can serve the function of precursor materials will undergo hydrolysis of and poly

condensation processes to form M-O-M bonds. In the hydrolysis process, as the name suggests, the precursor will hydrolyze and attains a hydroxyl group typically through the reaction with water. Poly-condensation is the process in which hydrolyzed species combine to make inorganic polymer-like chains through the elimination of a water molecule. The sol-gel synthesis process of nanoparticles was released to form inorganic compound through chemical reaction of a certain solution. The benefits of using sol-gel method are that it generates a good rate of thermal stability, high mechanical stability, good solution resistance, and possibility to stimulate transformation (Parihar et al., 2018).

2.7.Characterization techniques of Zinc Oxide nanoparticles (ZnO-NPs)

To apply zinc oxide nanoparticles (ZnO-NPs) for any of the applications characterizations should be held after the synthesis of the material. Several physical techniques have been developed to characterize the size, morphology, and other remarkable properties of zinc oxide nanoparticles (ZnO-NPs). The most commonly used characterization techniques are X-ray diffraction (XRD), UV-visible (UV-Vis) Spectroscopy, Fourier Transform Infra-Red (FTIR) Spectroscopy, and Photoluminescence (PL) Spectroscopy.

2.7.1. X-ray Diffractometer (XRD)

X-ray diffraction (XRD) is a powerful nondestructive technique for characterizing crystalline materials. It provides information on structures, phases, preferred crystal orientations (texture), and other structural parameters, such as average grain size, crystallinity, strain, and crystal defects. X-ray diffraction peaks are produced by constructive interference of a monochromatic beam of X-rays scattered at specific angles from each set of lattice planes in a sample. The peak intensities are determined by the distribution of atoms within the lattice. Consequently, the X-ray diffraction pattern is the fingerprint of periodic atomic arrangements in a given material (Bunaciu & Aboul-enein, 2015). The X-ray diffraction (XRD) technique has been used in this study to characterize the crystalline structure of the powder samples; the XRD also provided information on unit cell dimensions. It is an efficient non-destructive analytical technique used for the identification of the crystalline structure of compounds by their diffraction pattern. A diffraction pattern is produced when a material is irradiated with a collimated beam of x-rays. In the X-ray source, fast-moving electrons are bombarded at the target metal (usually Cu or Mo) to generate X-

ray as well as heat upon the rapid deceleration of electrons. The x-ray spectra generated by this technique provide a structural fingerprint of the material (unknown). The relative peak height is generally proportional to the number of grains in a preferred orientation and peak positions are reproducible.

XRD works on the principle that waves interacting with atomic planes in a material to form a diffraction pattern that is characteristic of the material's structure. Furthermore, XRD analysis can easily detect the existence of defects in a particular crystal, its resis- tance level to stress, its texture, its size and degree of crystal linity, and virtually any other variable relating to the sample's basic structure (Bunaciu & Aboul-enein, 2015).

2.7.2. Ultraviolet-visible spectroscopy (UV-Visible)

UV-visible Spectroscopy is the type of absorption spectrophotometer which involves the excitation of electrons present in the molecule from the ground state to the excited state. It is the most reliable and accurate analytical method used to measure the scanning or transition of electron and optical properties of materials. An absorption spectrophotometer is an analytical technique in which compounds absorb light of radiation of a specific wavelength. UV-Vis spectroscopy is almost entirely used for quantitative analysis in which the estimation of the amount of a compound known to be present in the sample solution. The absorption spectra of atoms, molecules, or ions are generated when a beam of electromagnetic energy or light is passed through a sample and absorbs a portion of the photons of electromagnetic energy passing through the sample.

The absorption peak depends on some factors like selection of wavelength, nature of the solvent, bandgap, oxygen deficiency, size and structure of the nanoparticles, surface roughness, impurity centers, PH of the solution, and temperature. The bandgap energy, the energy required for the transition of an electron from a state of lower energy (E_1) to the state of higher energy (E_2) is equivalent to the energy of electromagnetic radiation (photon energy) that causes transition. The bandgap energy can be determined by substituting the value of the absorption peak at a given wavelength in the following Eq (2.13) (Salahuddin et al., 2015):

$$E_g = E_2 - E_1 = h\nu = h\frac{c}{\lambda} = \frac{1.240}{\lambda_{\max}}\left[keV\right] \tag{2.13}$$

where Eg is the bandgap energy (eV), h is Planck's constant (4.135667×10^{-15} eVs), c is the velocity of light (3×10^{8} m/s), and λ is the wavelength (nm) of absorption onset.

The optical bandgap Eg is determined from a Tauc-plot from the following Eq (2.14) (Raj et al., 2017)

$$\alpha h\nu = A\left(h\nu - E_g\right)^n \tag{2.14}$$

where α is absorption coefficient, h is the Plank's constant, ν is the frequency of light radiation and Eg is the bandgap energy where 'n' takes the value of $1/2$ allowed direct transition.

2.7.3. Fourier Transformed Infra-Red (FTIR) Spectroscopy

FTIR Spectroscopy is a non-destructive and highly flexible instrument which able to measure bond vibrational motions of atoms in molecules. It is a powerful technique for chemical characterization, identification of functional groups and used to achieve information regarding the attachment of the capping agents. In recent times, it has been replaced with dispersive instruments for most applications due to its superior speed and sensitivity. The vibrational motion of atoms in a molecule is influenced by the masses of atoms, their geometrical arrangement, and the strength of their chemical bonds.

2.7.4. Photoluminescence (PL) Spectroscopy

Photoluminescence (PL) corresponds to the luminescence resulting from the transitions of energy states in the material excited by electromagnetic radiation. When a material is irradiated by light with significant energy, photons are absorbed and electrons are excited to higher energy levels (excited states). Eventually, the electrons return to the lower energy states (equilibrium states), and the excess energy is released as photoluminescence or non-radioactively (e.g. phonons).

2.8.Applications of Zinc Oxide nanoparticles (ZnO-NPs)

Zinc oxide nanoparticles (ZnO-NP) recently have received much attention due to various applications such as UV absorption, deodorization, and antibacterial treatment (Moballegh, 2007). The synthesis of Zinc oxide nanoparticles (ZnO-NPs) through the different modes leads to the development of nanostructures with novel properties. These novel properties such as optical, structural, electrical, morphological, properties are prominently dependent on surface Plasmon and quantum confinement effect. Overall, Zinc oxide nanoparticles (ZnO-NPs) are of importance for fundamental research, and also relevant for various fields of industrial and high technological applications (Karakız et al., 2008).

2.9.Antibacterial applications of Zinc oxide nanoparticles (ZnO-NPs)

In this review, consolidate all the information regarding zinc oxide nanoparticles as an antibacterial agent has been attempted. The mechanism of interaction of zinc oxide nanoparticles against a variety of microbes has also been discussed in detail.

Metal oxides with antimicrobial activity include iron oxide (Fe_3O_4), titanium dioxide (TiO_2), copper oxide (CuO), and zinc oxide (ZnO). Amongst, ZnO has been studied widely in the literature for its antimicrobial activity. ZnO is also approved by the Food and Drug Administration (FDA) and listed as a generally recognized as safe (GRAS) material for its antimicrobial activity and low toxicity to the host and it is shown to be effective as a food additive.

It is universally known that zinc oxide nanoparticles (ZnO-NPs) are antibacterial and inhibit the growth of microorganisms by permeating into the cell membrane. Oxidative stress damages lipids, carbohydrates, proteins, and DNA (Siddiqi et al., 2018). Zinc oxide nanoparticles (ZnO-NPs) have been used as an antibacterial substance against Salmonella typhi and S. aureus in vitro. Of all the metal oxide nanoparticles studied thus far, zinc oxide nanoparticles exhibited the highest toxicity against microorganisms.

Surface modification and functionalization are other factors leading to potential changes in NPs antimicrobial activity. Some functionalization can increase the presence of oxygen atoms on NPs surfaces that can lead to more reactive oxygen species (ROS) production in the medium. Releasing ions from NPs as a result of NP modification is possible, which consequently increases NP antimicrobial activity through the ion toxicity mechanism. In addition, NP modification can lead to an increase of the surface area, and thus it increases the surface-area-to-volume ratio that results in increasing the NP antimicrobial potential. Coating NPs is one of the modification approaches, which may be lead to the presence of more toxic agents or enhances one of the antimicrobial mechanisms of NPs, and also induces surface defects (such as vacancy defects) in the NPs (Hoseinzadeh et al., 2017).

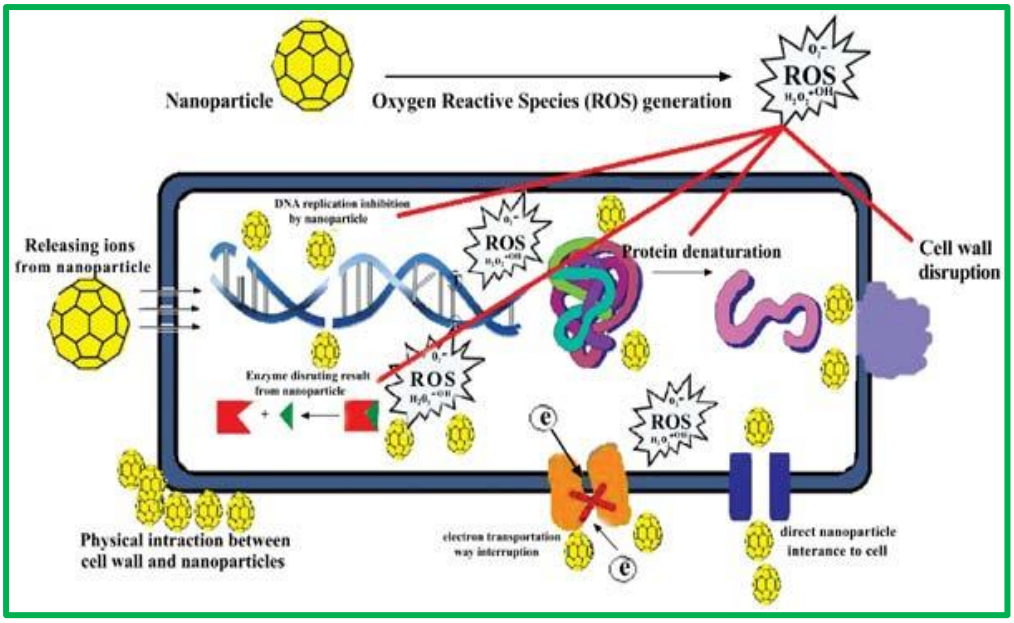

Figure 2.2: ROS and other mechanisms of antimicrobial activity of the metal NPs (Hoseinzadeh et al., 2017)

2.10. Probable Photodegradation Mechanism

The photodegradation mechanism of Methylene Blue (MB) carried out using Zinc oxide nanoparticles (ZnO-NPs) and Europium (Eu^{3+}) ion-doped Zinc oxide nanoparticles (ZnO-NPs) has been illustrated in Figure 2.3. Rare-earth elements (REE) can trap photoinduced electrons, thereby reducing the recombination of the electron-hole pairs (Labhane et al., 2018).

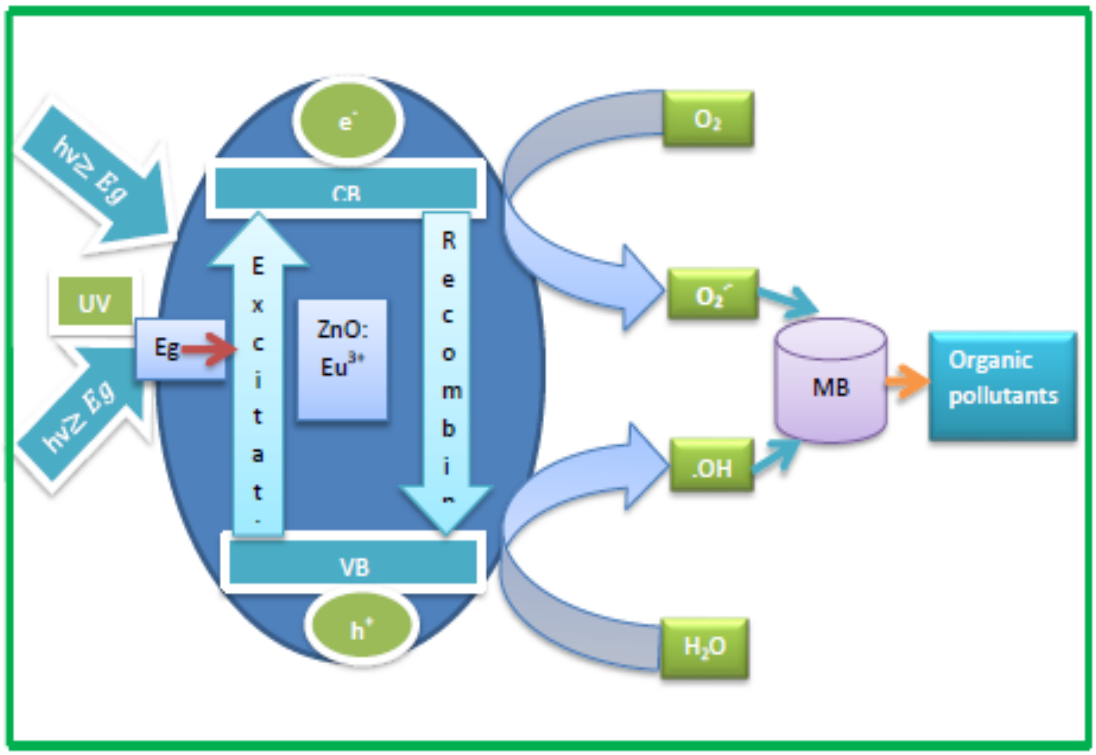

Figure 2.3: Possible mechanism of photocatalysis

ZnO is an n-type semiconductor that has very rich defect chemistry due to the presence of dominant electrons contributed by the oxygen vacancies and Zn interstitials (Habib et al., 2021). In the ZnO hexagonal wurtzite structure, the Zn atom occupies half of the tetrahedral sites leaving the octahedral site empty. This shows that ZnO is highly capable of accommodating both intrinsic defects and extrinsic dopants (Habib et al., 2021). The overall photo-degradation mechanism depends on the degree of the MB dye adsorption on the surface of the photocatalyst.

The photocatalytic process usually involves three steps: (1) the absorption of photons with energy larger than the band gap of a photocatalyst, (2) the generation, separation, migration, or recombination of photogenerated electron-hole pairs, and (3) the redox reactions on the photocatalyst surface (Zhang et al., 2016).

The photocatalytic process begins by excitation of holes (h^+) from the valence band to the conduction band of the ZnO semiconductor material, leaving behind the photo-generated electron (e^-) at the conduction band upon UV light irradiation. In photocatalytic activity, photons are absorbed by a photocatalyst, which then excites electrons from the valence to conduction bands to generate electron-hole pairs. The electron-hole pairs will react with surface-bound water to form hydroxyl radicals or

react directly with dye molecules (Nano-tio, 2015). These reactions can be represented by the following equations (Korake et al., 2014).

$$ZnO + h\nu \rightarrow ZnO\left(h_{VB}^{+} + e_{CB}^{-}\right) \quad (2.15)$$

$$e_{CB}^{-} + O_2 \rightarrow {}^{\bullet}O_2^{-} \quad (2.16)$$

$$h_{VB}^{+} + H_2O \rightarrow H^{+} + OH^{\bullet} \quad (2.17)$$

$$O_2^{\bullet} + H^{+} \rightarrow HO_2^{\bullet} \quad (2.18)$$

$$2e_{CB}^{-} + O_2 + 2H^{+} \rightarrow H_2O_2 \quad (2.19)$$

$$HO_2^{\bullet} + HO_2^{\bullet} \rightarrow H_2O_2 + O_2 \quad (2.20)$$

$${}^{\bullet}O_2 + HO_2^{\bullet} + H^{+} \rightarrow H_2O_2 + O_2 \quad (2.21)$$

$$MB + {}^{\bullet}OH / h_{VB}^{+} / {}^{\bullet}O_2^{-} \rightarrow Intermediates \rightarrow Degradation\ \text{Products} \rightarrow CO_2 + H_2O \quad (2.22)$$

A possible mechanism for the enhanced photocatalytic degradation of MB by the Europium (Eu^{3+}) ion-doped Zinc oxide nanoparticles (ZnO-NPs) photocatalyst was proposed as follows. The Europium (Eu^{3+}) ion-doped Zinc oxide nanoparticles (ZnO-NPs) particles could be excited by visible light ($\lambda \geq 380$ nm) to produce photogenerated electrons and holes (Equation 2.23). The rare earth elements (Eu^{3+}) dopant in Europium (Eu^{3+}) ion- doped Zinc oxide nanoparticles (ZnO-NPs) would serve as electron traps that could capture excited electrons (Equation 2.24) and facilitate the separation of electron-hole pairs, thus promoting the charge transfer from the bulk Zinc Oxide to the surface of the photocatalyst.

As a result, the photoinduced electrons transferred from the Eu^{3+} dopant to the photocatalyst surface could capture the adsorbed O_2 and reduce it to $O_2^{\bullet -}$ (Equation 2.25), and the formed $O_2^{\bullet -}$ would further participate in the MB degradation reactions (Equation 2.27. Simultaneously, the photogenerated holes after transporting to the photocatalyst surface could also react with H_2O to form ${}^{\bullet}OH$ (Equation 2.26) for the degradation of MB (Equation 2.27) or directly oxidize MB (Equation 2.27). According to the trapping experiments, holes, and superoxide radicals were believed to be the predominant reactive species for MB degradation (Equations 2.27), while

hydroxyl radicals could also play minor roles in the degradation process (Equation 2.27). Eventually, the organic pollutant could be mineralized into CO_2, H_2O (Zhang et al., 2016). Therefore, the proposed photocatalytic mechanism of Europium (Eu^{3+}) ion-doped Zinc oxide nanoparticles (ZnO-NPs) for MB degradation could be explained as follows (Zhang et al., 2016).

$$Zn_{(1-X)}Eu_{(x)}O + hv \rightarrow h_{VB}^{+} + e_{CB}^{-} \quad (2.23)$$

$$e_{CB}^{-} + Eu\,(dopant) \rightarrow e_{CB}^{-}(Eu\ dopant \quad trapped) \quad (2.24)$$

$$e_{CB}^{-}(Eu\ dopant \quad trapped) + O_2 \rightarrow O_2^{\bullet -} \quad (2.25)$$

$$h_{VB}{}^{+} + H_2O \rightarrow \bullet OH \quad (2.26)$$

$$MB + h_{VB}^{+\bullet} / O_2^{-} / {}^{\bullet}OH / \rightarrow Intermediates \rightarrow Organic Pollu\tan ts \rightarrow CO_2 + H_2O \quad (2.27)$$

3. MATERIALS AND METHODS

In this chapter, the materials and methods of the experiment were discussed in detail. The various chemicals, instruments, solvents necessary to carry out this work were also briefly elaborated. And also, the methods of Zinc Oxide nanoparticles (ZnO-NPs) for antibacterial and photo-catalytic activities were presented broadly.

3.1.Chemicals and solvents

The chemicals required for synthesizing ZnO Nanoparticles was: Zinc nitrate hexahydrate ($Zn(NO_3)_3 .6H_2O$) (New Delhi, India, assay; ≥99.6 %), Europium (III) nitrate pentahydrate ($Eu(NO_3)_3 .5H_2O$) (Sigma, Aldrich, USA, assay; ≥99.9%), Sodium Hydroxide (NaOH) (Alpha Chemica, India), and Methylene blue (MB). Ethanols, distilled water (DIW) have been used as solvents in this work. All the solvents used in the experiments were in analytical grade and used without any further purification.

The media required for culturing and antimicrobial tests were: Dimethyl Sulfoxide (DMSO) (Unichem, India, assay; ≥99%), M*ü*ller Hilton Agar (MHA) (M173-500G Himeda, Titan BIOTECH LTD. India), Tryptone Soya Agar (TSA) (T131-500G HiMedia, India), Nutrient broth ((M173-500G Himeda, India), and Ceftriaxone (positive control).

3.2.Apparatus and Instruments

3.2.1. Apparatus

The laboratory apparatus used for synthesizing the ZnO Nanoparticle using selective the co-precipitation method was: magnetic stirrer with a hot plate (ML 2lt), Different sizes of beakers, Thermometer, Filter papers (Wat-Mann-1) (size 110 mm), Digital electrical analytical balance (Model-FA2104, China), Furnace (Model- BK -5-12GJ, Biobase- Biodustry Co.Ltd., China), Ceramic crucible cups, Drying Oven (Model-DGH-9055, Jangasu Gangdu Mechanic Electronic Equipment Co Ltd., China), Pipettes, Cylinders, photo-reactor, pipettes, sample holders (tubers), and centrifuge.

The laboratory apparatus used for culturing bacterial strains were: Petri plates dishes (Gloves), Aluminum foils, Incubator, Test tubes, Rulers, Refrigerators, Cotton swab, Sterilizer.

3.2.2. Instruments

The laboratory instruments used for characterizing the ZnO Nanoparticle were: X-ray Diffraction (XRD) (XRD-700 X-RAY DIFFRACTOMETER MAXIma, SHIMADZU Corporation. Japan), UV-Visible (UV-Vis) Spectroscopy (DOUBLE BEAM SPECTROPHOTOMETER S-1600 SPECTROPHOTOMETER, India), Fourier Transformed Infra-Red Spectroscopy (FITR) (Perkin Elmer, Spectrum 65 FT-IR), and Photoluminescence (PL) (Model, MY18490002, Cary Eclipse, Fluorescence Spectrophotometer, Agilent Technologies, Malaysia), Ultrasonic bath, and photo-reactor.

3.3.Synthesis of Undoped and Europium (Eu^{3+}) ion- doped Zinc Oxide nanoparticles (ZnO-NPs)

To carry out the synthesis of undoped and Europium (Eu^{3+}) ion doped zinc oxide nanoparticles ((ZnO-NPs)) ($Eu_{1-x}Zn_xO$) (x= 0.00, 0.03, 0.06, 0.09) were prepared via co-precipitation method using zinc nitrate hexahydrate as precursors, Europium nitrate pentahydrate as dopant agent, and Sodium hydroxide (NaOH) as a precipitating agent as shown in a schematic diagram Figure 3.1 respectively. 0.57 M of zinc Nitrate hexahydrate were dissolved in 100 ml of deionized water. Then, 1 M of Sodium hydroxide (NaOH) was also dissolved in 100 ml of deionized water in a separate beaker. Then, the aqueous solutions of NaOH were added to the solutions of zinc nitrate hexahydrate in a dropwise manner and /or homogenously then stirred by magnetic stirrer continuously for 40 minutes at room temperature. Later, the prepared solutions were placed at room temperature for 3 hrs for the precipitation to occur. In this case, the white-colored precipitates were formed in the reaction mixtures. To separate the formed precipitates, the mixtures were then filtered with a What-man-1 filter paper size of 110 mm and rinsed several times (five times) with distilled water and ethanol to remove the possible ions remaining in the products (impurities). After the completion of the filtration, the residue was collected from the filter paper and then dried in a hot air oven at 80℃ for 19 hrs (overnight). The obtained Nanoparticles were milled (crushed) by an agate mortar and pestle to obtain pure ZnO NPs. After which the prepared Nanoparticles were annealed in a muffle furnace at 500℃ for $2\frac{1}{2}$ hrs. Finally, the prepared nanopowders were used for further investigations as usual.

Similarly, for the synthesis of $Zn_{0.91}Eu_{0.09}O$, $Zn_{0.94}Eu_{0.06}O$, $Zn_{0.97}Eu_{0.03}O$ NPs, the percentage amount of Europium nitrate pentahydrate ($Eu(NO_3)_3 .5H_2O$) must be known. So far, the percentage of composition of the starting materials ($Eu(NO_3)_3 .5H_2O$) in the evaporant mixtures were determined and described by the following method developed by (Jeetendra et al., 2014).

Thus, the method developed earlier has been written in the following ways:

$$Weight\%\ \left(\mathrm{Eu}\left(\mathrm{NO_3}\right)_3.5H_2O\right)=\frac{Weight\%\ \left(\mathrm{Eu}\left(\mathrm{NO_3}\right)_3.5H_2O\right)}{Weight\%\left(\mathrm{Eu}\left(\mathrm{NO_3}\right)_3.5H_2O\right)+Weight\%\left(\mathrm{Zn}\left(\mathrm{NO_3}\right)_3.6H_2O\right)}\times 100\%$$

(3.1)

Where $Weight\%\left(\mathrm{Eu}\left(\mathrm{NO_3}\right)_3.5H_2O\right)$ are weights of Europium nitrate pentahydrate ($Eu(NO_3)_3 .5H_2O$) in gram (gm), with distinct concentrations of Europium nitrate pentahydrate ($Eu(NO_3)_3 .5H_2O$) (x=0.00, 0.03, 0.06, 0.09) was used as a starting material for the synthesis of Europium (Eu^{3+}) ion-doped with Zinc Oxide nanoparticles (ZnO-NPs). In doing so, for the synthesis of distinct concentrations of Europium nitrate pentahydrate ($Eu(NO_3)_3 .5H_2O$) using the above developed method, i.e., (x=0.03) (0.619 gm), (x=0.06) (1.276 gm), and (x=0.09) (1.979 gm) were dissolved in 100 ml of distilled water. Here the solutions contain the dopant material was preferred in between them while the three solutions were added dropwise by using the micro-pipettes. Similar procedures were adopted to synthesize Europium (Eu^{3+}) ion-doped Zinc Oxide nanoparticles (ZnO- NPs) with different concentrations of Europium nitrate pentahydrate (x=0.00, 0.03,0.06,0.09) remains as of Undoped Zinc Oxide nanoparticles (ZnO-NPs) as said above.

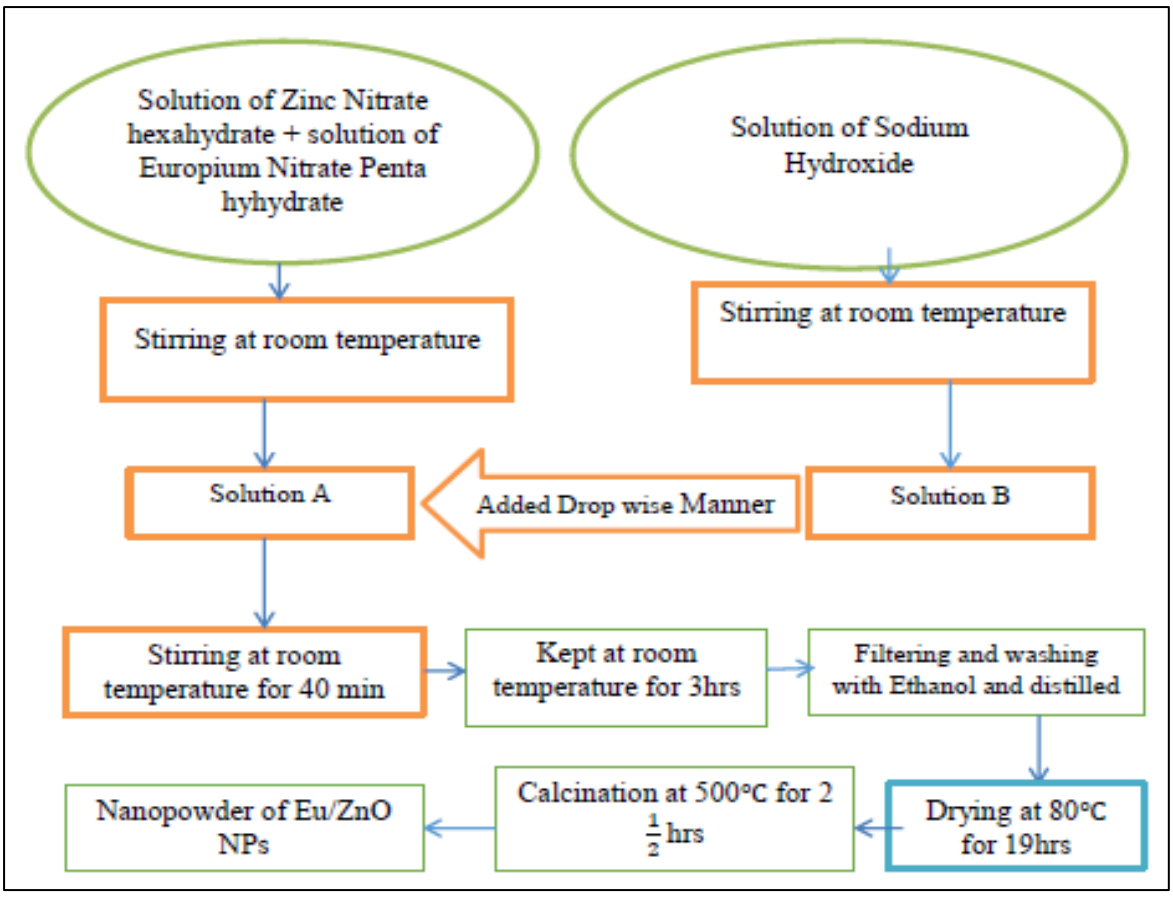

Figure 3.1: Plausible illustration of synthesis of Eu3+ ion- doped Zinc Oxide nanoparticles (ZnO- NPs)

3.4.Characterization Techniques

The X-ray diffraction pattern of ZnO Nanoparticles was recorded on (X-RAY DIFFRACTOMETER MAXIma) which is equipped with Cu-Kα_1 radiation (λ=0.154056 nm) and operates at a voltage of 40 kV and applied current of 30 mA in the scanning speed of 3.00 degrees per minutes which in turn the collected data were scanned at a range of 2θ=10° $\leq 2\theta \leq$ 80°. This X-ray diffractometry is used to determine the plane spacing, crystalline size, lattice parameters, bond length, positional parameters, dislocation density, and micro- strain of Undoped, and Europium (Eu^{3+}) ion-doped ZnO Nanoparticles by using the relation expressed in Eqs (2.2- 2.12).

The UV-Vis absorption peaks of ZnO NPs were recorded with UV-Vis spectroscopy (DOUBLE BEAM SPECTROPHOTOMETER S-160 SPECTROPHOTOMETER) in the wavelength region of 200-600 nm at room temperature. The Undoped and Europium (Eu^{3+}) ion–doped Zinc Oxide nanoparticles (ZnO-NPs) were dissolved in

DMSO and then its absorbance is measured using a 1cm quartz cuvette. The ASCII files of the measured spectra were collected by a computer that interfaced with the instrument. Finally, the absorption spectra of Undoped and Europium (Eu^{3+}) ion-doped Zinc Oxide nanoparticles (ZnO-NPs) were analyzed using Origin 8 software. The absorption peak, energy bandgap of doped ZnO nanoparticles and calculated using Eqs (2.13-2.14).

The emission spectra of Undoped and Europium (Eu^{3+}) ion-doped Zinc Oxide nanoparticles (ZnO-NPs) were measured with Fluorescence Spectroscopy (Cary Eclipse, Fluorescence Spectrophotometer) at room temperature. Before the measurements, the NPs samples were dissolved in di-methyl sulphoxide (DMSO) with equal measurements by Digital electrical analytical balance and stirred until it dissolved. After it is dissolved in DMSO, it is filtered with Watt-Mann filter paper in proper measurements of the samples. The emission spectra of the sample were measured by a 1 cm quartz cuvette. The excitation wavelengths of the samples were monitored at 325, 380, and 394 nm respectively for Undoped and Europium (Eu^{3+}) ion-doped Zinc Oxide nanoparticles (ZnO-NPs), and the emission wavelength was measured at a wavelength range of 350-600, 400-650 nm respectively. Finally, the slit width of the instrument was adjusted to 10 nm.

The functional groups attached to the nanoparticles were also measured by Fourier Transform Infra-Red Spectroscopy (Perkin Elmer, Spectrum 65 FT-IR) in the wavenumber region of 4000-400 cm^{-1}. The FT-IR spectra measurements of the NPs were analyzed by putting the powder of Undoped and Europium (Eu^{3+}) ion-doped Zinc Oxide nanoparticles (ZnO-NPs) on the KBr pellets.

The photo-degradation efficiency of Undoped and Europium (Eu^{3+}) ion-doped Zinc Oxide nanoparticles (ZnO-NPs) were evaluated by the degradation of methylene blue in aqueous solutions under UV light in the time interval of 0-60 min and finally, the absorption spectra were determined by scanning the wavelength from 200 nm-800 nm.

3.5.Determination of antibacterial test of undoped and Europium (Eu^{3+}) ion-doped Zinc Oxide nanoparticles (ZnO-NPs)

The antimicrobial activity of Undoped and Europium (Eu^{3+}) ion-doped Zinc Oxide nanoparticles (ZnO-NPs) with different bacterial species of interest gram-positive

bacteria (*Staphylococcus aureus (S. aureus))* (ATCC-25923) and gram-negative bacteria (*Escherichia coli, E.coli*) (ATCC-25922) was determined using the agar disc diffusion method (Belay, 2017). Microbial strains were grown in nutrient broth aerobically at 37°C for 24 hrs until the turbidity of bacterial suspensions achieved to 1.5 x10^8 CFU mL^{-1} by comparison with the 0.5 Mc Farland standards. 0.01 ml of each sub-cultured bacteria and yeast test organism were spread using a sterilized cotton swab on 20 mL of sterilized molten and cooled MHA media and TSA media, respectively. Subsequently, agar wells of 6mm diameter were impregnated on different plates with a sterilized stainless steel cork borer and labeled properly. Different concentrations of Undoped and Europium (Eu^{3+}) ion-doped Zinc Oxide nanoparticles (ZnO-NPs) (100, 150, and 200 µg/ml) of solutions were added into disc-using micropipette. The plates containing the microbes and nanoparticles were incubated at 37°C for 24 hrs in the case of bacteria before measuring the zone of inhibition.

After incubation, the plates were examined for a clear zone around the discs or wells. The diameter of such zones of inhibition was measured using a ruler and mean values for each organism were recorded and expressed in millimeters and finally compared with the standard drug, Ceftriaxone.

3.6.Experimental procedure for the photocatalytic degradation of Methylene Blue

The photocatalytic activities of Undoped and Europium (Eu^{3+}) ion-doped Zinc Oxide nanoparticles (ZnO-NPs) were investigated by measuring the degradation of methylene blue (MB) in an aqueous solution under UV radiation. Precisely, the photocatalytic reactions were carried out in a transparent spherical glass reactor with 100 ml capacity.

Each 0.05g of Undoped and Europium (Eu^{3+}) ion-doped Zinc Oxide nanoparticles (ZnO-NPs) were poured into 100 ml of 10-ppm MB aqueous solutions, then the suspension was kept in magnetic stirring in an ultrasonic bath for 30 min to achieve the adsorption/desorption equilibrium of methylene blue on the surface of photocatalyst. The light was turned on to initiate the test. During the period of irradiation, the reaction mixture was continuously stirred at RT and 5ml aliquots were withdrawn from the suspensions at time intervals of 15 min until the final irradiation time of 60 min was achieved. After the completion of irradiation time, the mixtures

were centrifuged at 3000 rpm for 10 min to obtain the clean and homogenous samples. Finally, the solutions were subjected to the absorption spectrum measurements using the UV-visible (UV-3600Plus Series) spectrophotometer at a wavelength of 665 nm with the standard MB as a reference. According to Beer-Lambert Law, MB's concentration is directly proportional to its absorbance. This makes it possible to determine the oxidation efficiency of MB using the following Eq (3.2) (Amali et al., 2014).

$$\text{Decolorization efficiency (\%)} = \left[1-\left(\frac{C_t}{C_0}\right)\right]\times 100\% \qquad (3.2)$$

where C_0 is the initial concentration of MB solution and C_t is the concentration of MB during irradiation.

4. RESULTS AND DISCUSSION

In this chapter, the results and discussions of the experiments were presented. The first section of this chapter introduced the basic crystal structure as well the lattice parameters, strain-induced, dislocation density of Undoped and Europium (Eu^{3+}) ion doped with Zinc Oxide nanoparticles (ZnO-NPs). In the second section of this chapter, room temperature measurements of photoluminescence spectra with a different excitation wavelength of Undoped and Europium (Eu^{3+}) ion- doped with Zinc Oxide nanoparticles (ZnO-NPs) were discussed. In the third section of this chapter, the absorption spectra of Undoped and Europium (Eu^{3+}) ion- doped with Zinc Oxide nanoparticles (ZnO-NPs) were also clearly elaborated. In the fourth section of this chapter, the functional groups and their assignments of Undoped and Europium (Eu^{3+}) ion- doped with Zinc Oxide nanoparticles (ZnO-NPs) were presented briefly. In the fifth section of this chapter, antibacterial activity applied on Undoped and Europium (Eu^{3+}) ion-doped with Zinc Oxide nanoparticles (ZnO-NPs) was also stated. Finally, the photocatalytic activity of Undoped and Europium (Eu^{3+}) ion-doped with Zinc Oxide nanoparticles (ZnO-NPs) was also presented.

4.1.X-ray Diffraction (XRD) Analysis

X-ray diffraction measurements have been employed to analyze the crystalline size and the fundamental properties of Undoped Zinc Oxide nanoparticles (ZnO- NPs) and Europium (Eu^{3+}) ion-doped Zinc Oxide nanoparticles (ZnO- NPs). The inset of Figure 4.1 below clearly depicts that the X-ray diffraction patterns of undoped Zinc Oxide nanoparticles (ZnO- NPs) and Europium (Eu^{3+}) ion-doped Zinc Oxide nanoparticles (ZnO- NPs). The observed diffraction peaks were observed 31.8150°, 34.4768°, 36.3024°, 47.5913°, 56.6409°, 62.9131°, 63.2033°, 66.4186°, 67.9977°, 69.1311°, 77.0099° indexed to (100), (002), (101), (102), (110), (103), (200), (112), (201), and (202) planes. Thus, the samples clearly show the wurtzite structure of ZnO with hexagonal phase, and the observed peaks were fitted with the Joint Committee on Powder Diffraction Standard (JCPDS card No. 36-1451, space group P63mc, 186) (Badreddine et al., 2018). Moreover, the XRD pattern depicts that, sharp and intense peaks were observed, which shows that the prepared samples were highly crystalline.

It is noted that no other secondary phases such as Europium Oxides (Eu_2O_3) could be detected from the XRD reflection patterns which may be ascribed due to the successful incorporation of Eu^{3+} ion into the host ZnO crystal lattice. Similar trends have also been observed in the literature (Badreddine et al., 2018) (Vijayaprasath et al., 2015). The lower angle shift in diffraction peaks for (Eu^{3+}) ion-doped ZnO NPs was mainly caused by the dopant of Eu^{3+} ions substituted, as well as distortion in the host ZnO lattice crystal as well. It can be seen that, in the inset of Figure 4.2 below, while the doping concentration of Eu^{3+} ions is increased, it was clear that the peak corresponding to the most intense peak (101) XRD patterns related to ZnO shifted towards the lower angles side as shown in Figure 4.2.

This is evidence for the creation of internal compressive micro-stress in the doped samples. Similar changes by doping rare earth elements with ZnO Nps have been also reported in the work of (Naik et al., 2020) as well. Likewise, the other reason for the shift in peak intensity is that, the ionic radius mismatch that is occurred between Eu^{3+} ions and that of Zn^{2+} ions respectively. The ionic radius for Eu^{3+} is 0.095 nm and that of Zn^{2+} is 0.074 nm respectively. Meanwhile, the shift is also caused by the strain developed due to the effect of different ionic radii of the respective metal ions. Furthermore, the small amounts that were introduced into the Zn^{2+} interstitial sites are also playing a great role in the shifting of the diffraction peak positions. The decrease in intensity of ZnO diffraction peaks indicates that the lattice distortion is induced at higher Eu^{3+} ion concentrations and deteriorates the purity phase of crystallization of ZnO. Similar results also studied in the literature broadly (Xin, 2018).

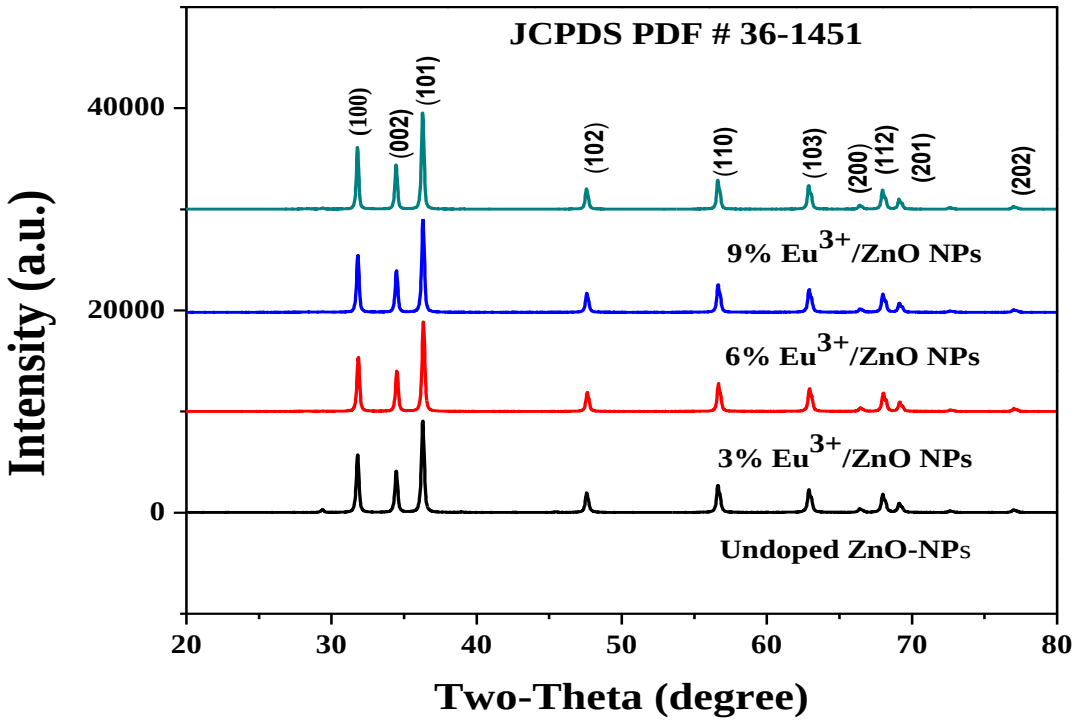

Figure 4.1: XRD Patterns of Undoped, $Zn_{0.97}Eu_{0.03}O$, $Zn_{0.94}Eu_{0.06}O$, and $Zn_{0.91}Eu_{0.09}O$ ZnO NPs

Table 4.1: Variation of crystallite size, micro strain, dislocation density, full width at half maximum, plane spacing of Undoped and Europium (Eu^{3+}) ion doped Zinc Oxide nanoparticles (ZnO- NPs)

S. No	Concentrations of Eu^{3+} (%)	Two theta of (101) (°)	D_{101} (nm)	d101(A)	FWHM (°)	Micro strain (10^{-4})	Dislocation density (lines per m^2)
1	0.00	36.3024	39.4	2.47267	0.20780	8.620	6.442E+14
2	0.03	36.3431	40.0	2.46999	0.20700	8.580	6.250E+14
3	0.06	36.3168	43.5	2.47172	0.18900	7.830	5.285E+14
4	0.09	36.2956	45.0	2.47312	0.18390	7.620	4.938E+14

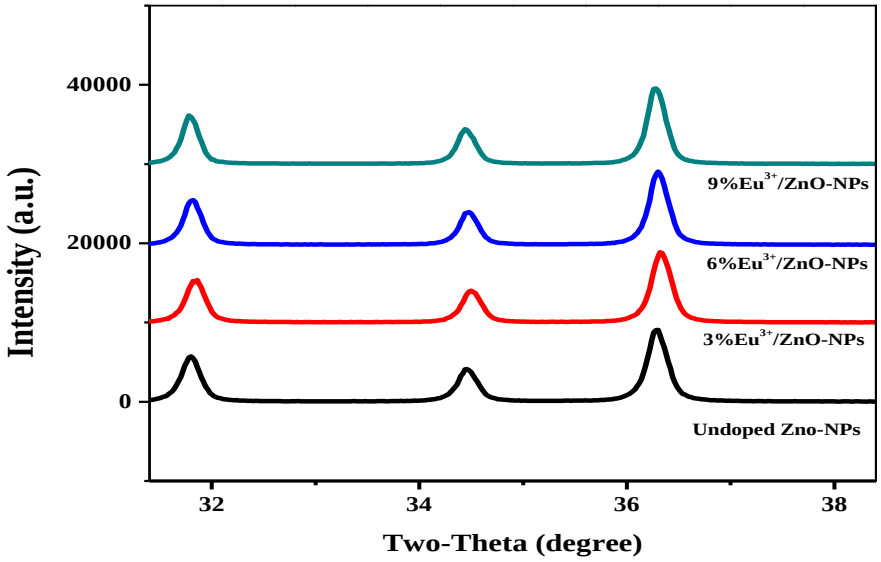

Figure 4.2: Peak shift analysis of Undoped, Undop, $Zn_{0.97}Eu_{0.03}O$, $Zn_{0.94}Eu_{0.06}O$, and $Zn_{0.91}Eu_{0.09}O$ ZnO NPs.

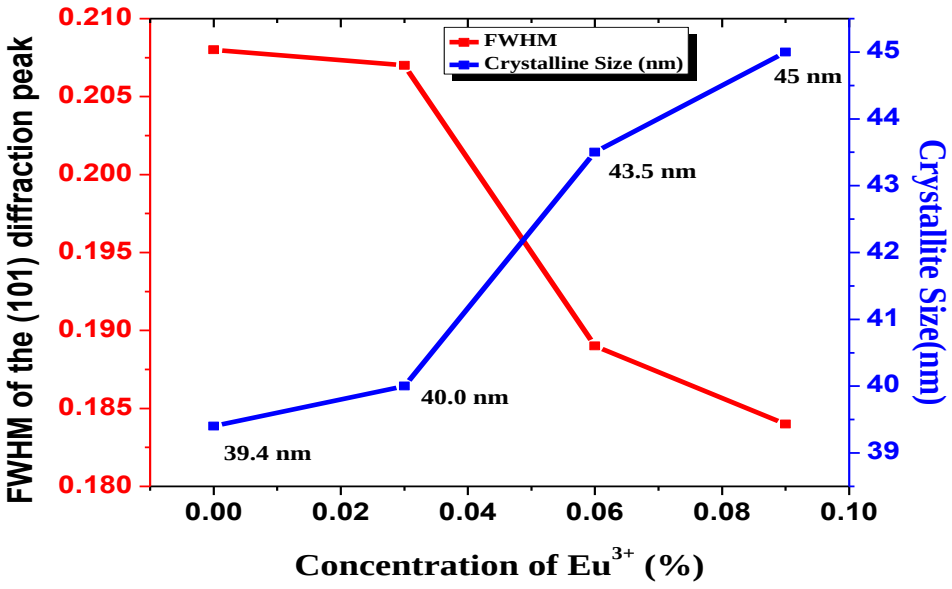

Figure 4.3: Plot of Full Width at Half Maximum (FWHM) and crystalline size for the most intense diffraction peak for undoped, $Zn_{0.97}Eu_{0.03}O$, $Zn_{0.94}Eu_{0.06}O$, and $Zn_{0.91}Eu_{0.09}O$ ZnO NPs.

Table 4.1 clearly shows the calculated and tabulated values of the crystallite size, micro-strain, and dislocation density from equations of (2.8-2.10) for Undoped Zinc Oxide nanoparticles (ZnO- NPs), $Zn_{0.97}Eu_{0.03}O$, $Zn_{0.94}Eu_{0.06}O$, and $Zn_{0.91}Eu_{0.09}O$ NPs respectively. The crystallite size of Undoped Zinc Oxide nanoparticles (ZnO- NPs) is estimated to be 39.4 nm. The crystallite size for $Zn_{0.97}Eu_{0.03}O$, $Zn_{0.94}Eu_{0.06}O$, and $Zn_{0.91}Eu_{0.09}O$ NPs increase when compared to undoped ZnO NPs as shown in Table 4.1. It is worth noting that the increase in the crystallite size is due to the distortion in a host ZnO lattice by the addition of foreign impurities and i.e. Eu^{3+} ion into host lattice sites, which in turn increases the nucleation and subsequent growth rate of ZnO NPs. In addition, from Figure 4.3, the increase in crystalline size when the concentration of Eu^{3+} ion increase is attributed to mainly the replacement of Zn^{2+} ions into the host ZnO crystal lattice. In the work of O.M. Ntwaeaborwa et al. (Ntwaeaborwa et al., 2017), the structure, particle morphology, and luminescent properties of europium (Eu^{3+}) ion-doped Zinc Oxide nanoparticles (ZnO- NPs) were prepared by the co-precipitation method are discussed. They predicted that the crystallite size values of both Undoped and Europium (Eu^{3+}) ion-doped Zinc Oxide nanoparticles (ZnO- NPs) were increases as the concentration of (Eu^{3+}) ion increases. The reduction in the micro-strain as the concentration of the sample is being increased from (x=0.00- 0.09) is mainly due to the compression strain in the crystal lattice of the particle size.

It is likewise intriguing to note that by further increase the concentration of doping level the diffraction peak sharpness goes to increase with the full width at half maxima (FWHM) value becomes lower from 0.208700-0.18390. Precisely, smaller FWHM means the progress of larger particle size. On this basis, there were enhancements of the crystallization process in the leads to the sharper diffraction peak.

Table 4.2.Variation of structural parameters of Undoped and Europium (Eu^{3+}) ion-doped Zinc Oxide nanoparticles (ZnO- NPs)

S. No	Lattice parameters (nm)		Atomic packing fraction	Volume $V(A°)^3$	Positional parameter	Bond length (Zn–O)	Atomic Packing Fraction
	a	c					

			(c/a)		er (u)	(L) (Å)	(APF) (%)
1	0.3245	0.5218	1.605	47.730	0.3790	1.977	75.16
2	0.3241	0.5193	1.602	47.240	0.3793	1.973	75.43
3	0.3243	0.5197	1.603	47.330	0.3797	1.974	75.42
4	0.3245	0.5200	1.602	47.420	0.3798	1.975	75.40

Calculated structural parameters such as lattice parameters, atomic packing factor, the volume of the unit cell, positional parameters, and bond length of Undoped and Europium (Eu^{3+}) ion-doped ZnO Nps using (2.4-2.7, 2.11) respectively for distinct concentrations are presented and tabulated in table 4.2 above. More importantly, it can be seen that the lattice parameters of semiconductors usually depend on the foreign atoms, and defects, and the difference in ionic radii for the substituted matrix ions. Furthermore, the increasing of the concentrations of Eu^{3+} ion-doped ZnO NPs causes the major change in the lattice parameters, atomic packing factor, volume of the unit cell, positional parameters, and bond length in all aspects.

.

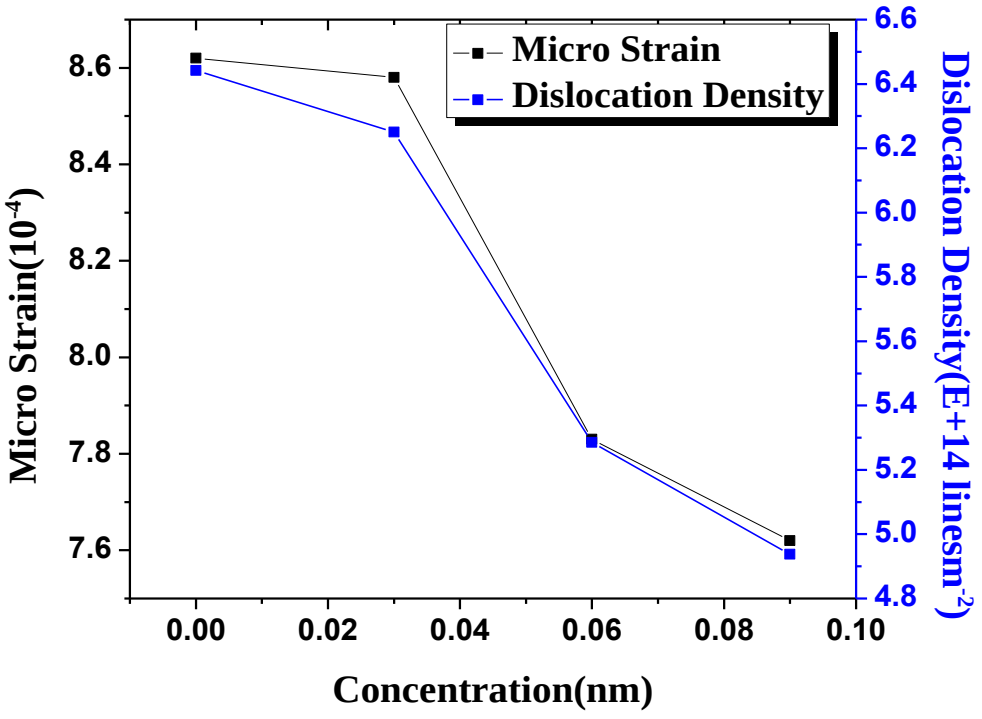

Figure 4.4: Effect of concentration of Eu^{3+} ion on micro strain and dislocation density

It can be seen that as the concentration of the Europium (Eu^{3+}) ion is increased from 0.00-0.09 with instep of 0.03, the prominent structural parameters of doped ZnO NPs significantly change from the conventional bulk counterpart of ZnO NPs. On the other hand, variations of lattice parameters such as 'a' and 'c' are reflected due to the shift of diffraction peak positions, which may depend on the difference in ionic radius between the main element and the dopant ion. Interestingly, the bond length values are found to increase with the increase in Europium (Eu^{3+}) ion concentrations as presented in table 4.2 above due to the effect of the replacement of Zn^{2+}ions in ZnO crystal lattice. It is noted that, as shown in Figure 4.4, as the doping concentration of Europium (Eu^{3+}) ion increases, the micro-strain, and the dislocation density decrease predominantly, which is ascribed due to the Europium (Eu^{3+}) ion doping inside the Zinc Oxide (ZnO) matrix which in turn causes the local distortion of the crystal structure. This is evidence that the doping process is an elegant method to vary the properties of the materials.

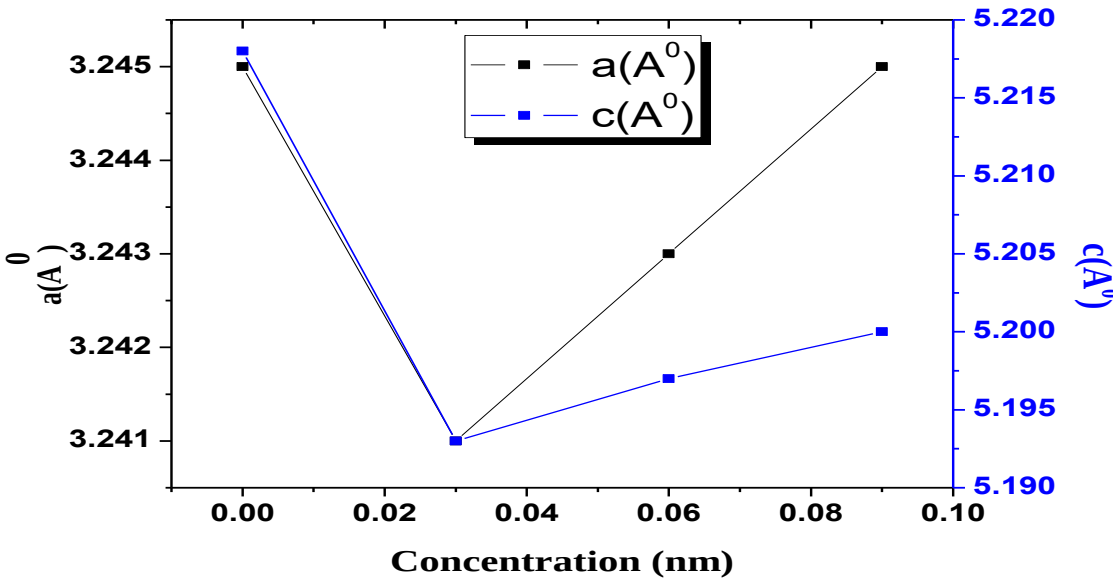

Figure 4.5: Effect of concentration of Eu^{3+} ion on lattice parameters

4.2.Ultra Violet Visible (UV-Vis) absorption spectra

Figure 4.6(a) depicts the Ultra Violet Visible (UV-Vis) absorption spectra of Undoped $Zn_{0.97}Eu_{0.03}O$, $Zn_{0.94}Eu_{0.06}O$, and $Zn_{0.91}Eu_{0.09}O$ ZnO NPs respectively. With further increase of Europium (Eu^{3+}) ion to the higher concentrations, there are minor shifts of wavelength. In our study, with the increase in the concentration of Europium (Eu^{3+})

ion, the energy bandgap compared to Undoped Zinc Oxide nanoparticles (ZnO-NPs) becomes increases which dominate the quantum confinement effect. Compared to Undoped Zinc Oxide nanoparticles (ZnO-NPs) the blue shift peaks were observed for the case of Europium (Eu^{3+}) ion-doping Zinc Oxide nanoparticles (ZnO-NPs). On the one hand, the observation of this study may be ascribed, according to the Burstein-Moss Effect (BME), this result holds, which mean that, with increase the concentration of dopant amount, the energy bandgap becomes widening which increases the Fermi level in the conduction band of degenerate host materials.

It is worth noting that, for Undoped Zinc Oxide nanoparticles (ZnO-NPs) and Europium (Eu^{3+}) ion doped Zinc Oxide nanoparticles (ZnO-NPs) the absorption peaks are found in the range of Ultra-Violet emission which happened when the electron transits from the valance band to the conduction band. The values of energy bandgap for Undoped Zinc Oxide nanoparticles (ZnO-NPs) and Europium (Eu^{3+}) ion doped Zinc Oxide nanoparticles (ZnO-NPs) were calculated from Eq (2.13) and tabulated in table 4.3.

It is also noted that when the concentration of Europium (Eu^{3+}) ion increase from (x=0.00-0.09%) the energy bandgap values increase from 3.26 eV-3.28 eV. The results also demonstrated that the Europium (Eu^{3+}) ion doping with varying the concentration has had a particular role in enhancing the energy bandgap of the synthesized materials as well. In this work, the incorporation of the (Eu^{3+}) ion into the ZnO matrix or the host semiconductor has been the main effect for the energy bands closer to the conduction band edges.

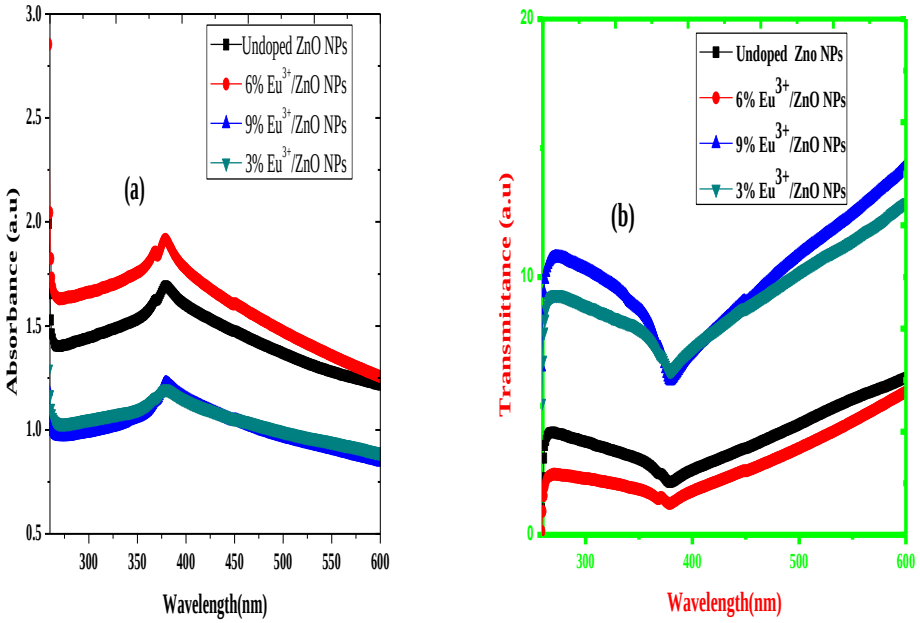

Figure 4.6(a) UV-Vis absorbance spectra and (b) UV-Vis transmission spectra of Undoped, and $Zn_{0.97}Eu_{0.03}O$, $Zn_{0.94}Eu_{0.06}O$, and $Zn_{0.91}Eu_{0.09}O$ ZnO NPs

Table 4.3: Calculated energy bandgap for Undoped, $Zn_{0.97}Eu_{0.03}O$, $Zn_{0.94}Eu_{0.06}O$, and $Zn_{0.91}Eu_{0.09}O$ ZnO NPs respectively.

S.No	Concentrations (%)	Maximum wavelength (λ_{max}) (nm)	Energy band gap Eg (eV)
1	0.00	381	3.26
2	0.03	379	3.27
3	0.06	380	3.26
4	0.09	378	3.28

Figure 4.6(b) illustrates the transmission versus wavelength of Undoped Zinc Oxide nanoparticles (ZnO-NPs) and Europium (Eu^{3+}) ion doped Zinc Oxide nanoparticles (ZnO-NPs).

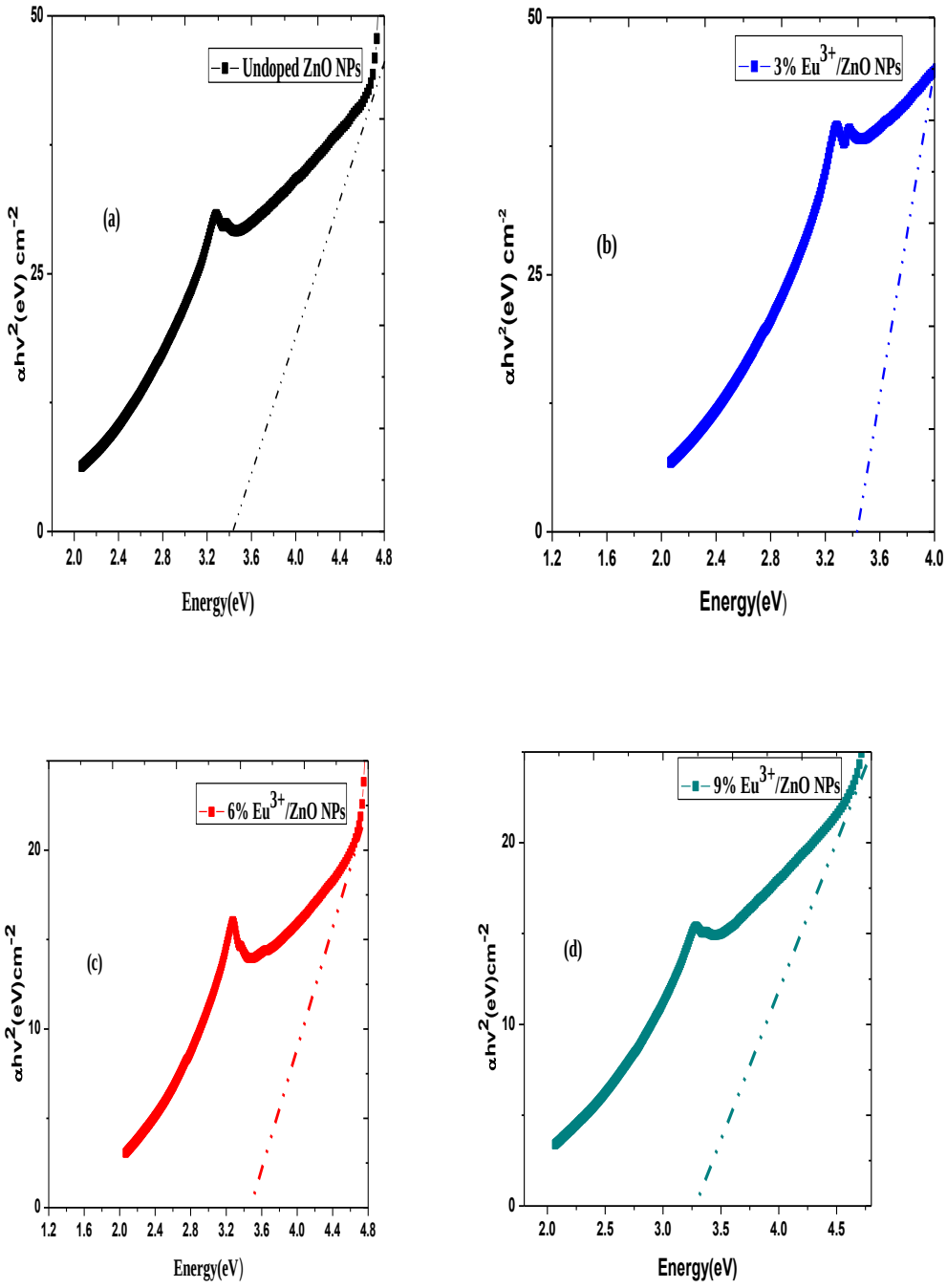

Figure 4.7: Tauc's pilots drawn $(\alpha hv)^2$ versus the energy (eV) of (a) Undoped (b) $Zn_{0.97}Eu_{0.03}O$, (c) $Zn_{0.94}Eu_{0.06}O$, and (d) $Zn_{0.91}Eu_{0.09}O$ ZnO NPs respectively.

Figure 4.7 above emphasizes the Taucs pilot of Undoped Zinc Oxide nanoparticles (ZnO-NPs) and Europium (Eu^{3+}) ion doped Zinc Oxide nanoparticles (ZnO-NPs). The $(\alpha hv)^2$ plot as a function of photon energy (eV) is displayed in the inset of Figure 4.7. The values of the energy bandgap are estimated from the

extrapolation of a straight line down to the $(\alpha hv)^2$ =0 and they vary from 3.26 eV-3.28 eV. It is intriguing to note that, the absorption edges of Europium (Eu^{3+}) ion-doped Zinc Oxide nanoparticles (ZnO-NPs) go to partially higher energy values which may be attributed due to the addition of dopant metal which is more activator rare earth elements (REE).

Previous reports suggest a small increase in the values of energy bandgap with further increase the doping concentration is consistent with the minor shifts in the peak intensity (blue shift) in the study of UV-Visible absorption spectra and displays the broadening of the bandgap with increasing the doping concentrations (Pal & Manam, 2013).

4.3.Photoluminescence Analysis

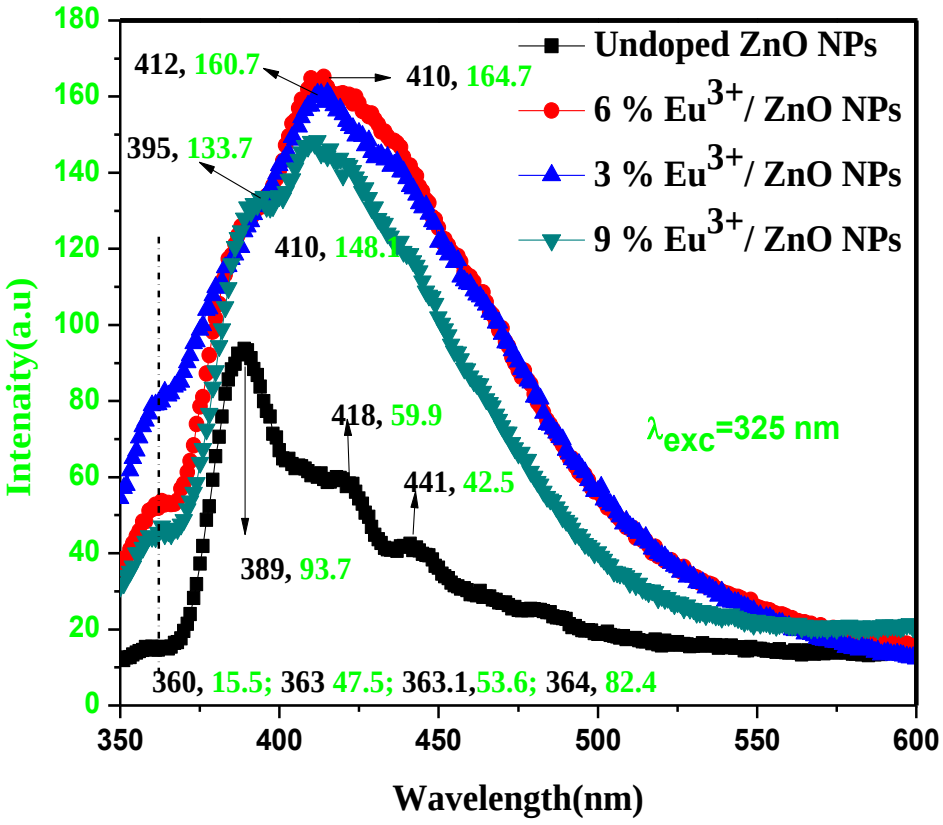

Figure 4.8: Room temperature photoluminescence emission spectra of Undoped, $Zn_{0.97}Eu_{0.03}O$, $Zn_{0.94}Eu_{0.06}O$, and $Zn_{0.91}Eu_{0.09}O$ ZnO NPs excited at a wavelength of 325 nm.

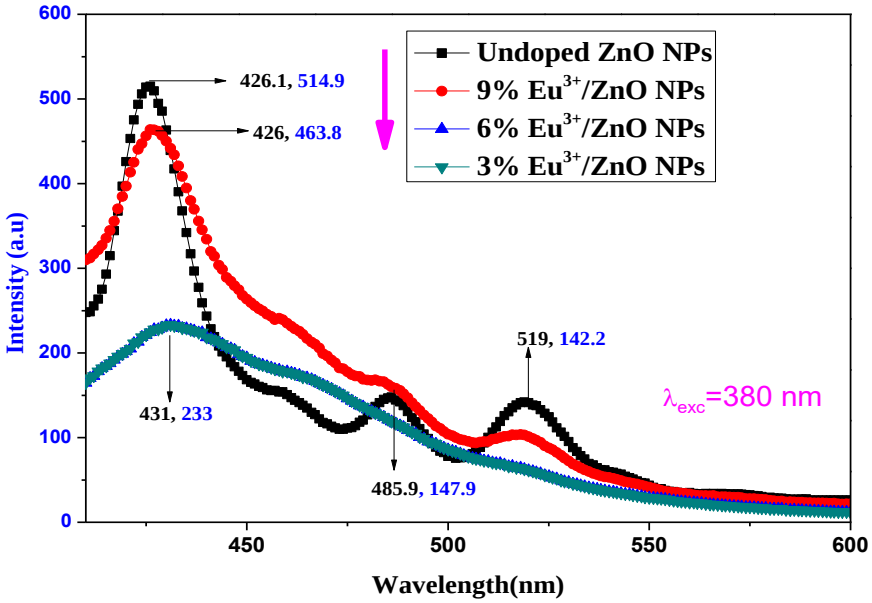

Figure 4.9: Room temperature photoluminescence emission spectra of Undoped, $Zn_{0.97}Eu_{0.03}O$, $Zn_{0.94}Eu_{0.06}O$, and $Zn_{0.91}Eu_{0.09}O$ ZnO NPs excited at a wavelength of 380 nm.

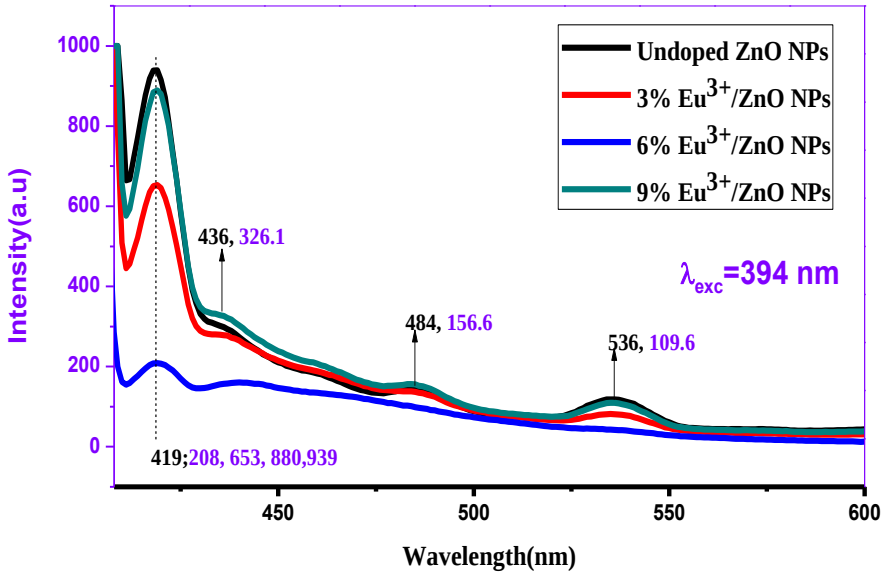

Figure 4.10: Room temperature photoluminescence emission spectra of Undoped, $Zn_{0.97}Eu_{0.03}O$, $Zn_{0.94}Eu_{0.06}O$, and $Zn_{0.91}Eu_{0.09}O$ ZnO NPs excited at a wavelength of 394 nm.

PL spectra of undoped and Europium (Eu^{3+}) ion-doped Zinc Oxide nanoparticles (ZnO-NPs) were obtained by exciting with the excitation wavelength of 325 nm 380, and 394 nm respectively at room temperature as shown in the inset of Figure (4.8)-(4.10). PL spectra show some peaks in the range of 361-441 nm, 427-518 nm, and 419-536 nm (both UV emission and visible regions) with the excitation wavelength of 325, 380, and 394 nm respectively. More importantly, a sharp peak observed at 388 nm is attributed to the band -to- band transitions are known as near band edge emission (NBE). For the excitation wavelength of 325 nm, the broad emission peak around 418 nm can be observed in Europium (Eu^{3+}) ion-doped Zinc Oxide nanoparticles (ZnO-NPs) also due to the strong UV emission which is attributed to the radiative recombination of excitons (exciton emission) i.e. electronic transitions from the conduction band to the valence band. Similar trends are also observed in the literatures (Xin, 2018) (Dash et al., 2019) (Ma & Wang, 2012)(Pal & Manam, 2013).

Moreover, the high intensity was obtained while the concentrations of Europium (Eu^{3+}) ion- doping were increases from (x=0.00-0.09) respectively. When the concentration of Europium (Eu^{3+}) ion is increased from (x=0.00-0.09) shifts in peaks position is occurred which in turn resulted that the photoluminescence emission predominantly depends on the concentration of Europium (Eu^{3+}) ion-doped. From fig (4.9-10), it can be seen that the strong emission peak is observed at 426 nm (~2.913 eV) and 419 nm (~2.961 eV) and transitions of $^7F_1 \rightarrow ^5D_3$ and $^7F_0 \rightarrow ^5D_3$ for an excitation wavelength of 380 nm and 394 nm respectively, which may be attributed due to the deep-level defect states in the Europium (Eu^{3+}) ion-doped ZnO Nps which due to oxygen vacancies and zinc interstitials. On doping of Europium (Eu^{3+}) ion-doped ZnO Nps, the peak intensity becomes decreased when excited at 380 nm than the intensity of undoped ZnO Nps. It is also imperative that the strain developed in the sample due to doping agents plays a major role in shifting the photoluminescence emission peak. It is apparent that from Figure (4.9) the series characteristics of emissions such as violet (431 nm) (~2.879 eV), blue (~485.9 nm) (~2.554 eV), and green emission (519 nm) (~2.400 eV) were observed. On the one hand, when excited at 394nm the peak intensity becomes increased while the concentration of Europium (Eu^{3+}) ion-doped Zinc Oxide nanoparticles (ZnO-NPs) is increased.

In doing so, as it can be seen in Figure (4.10) the series characteristics of emissions such as violet (437 nm) (2.840 eV), blue 486 nm) (~2.553 eV), and green emission (536 nm) (~2.315 eV) was observed when excited at 394 nm. Those various series characteristics were observed due to the doping effect of Europium (Eu^{3+}) ion into the host Zinc Oxide Nanoparticles (ZnO-NPs). Further, the blue emissions have arisen as a result of the recombination of zinc interstitial energy level to zinc vacancy energy level and that of green emission is occurred due to the recombination of singly ionized oxygen vacancies. Certain groups have also indicated the same trends as well (Choudhary, 2020)(Koao et al., 2016). The emission peaks observed at 485, 518, 486, and 536 nm were found to be extremely weak for wavelength excitation of 389 nm and 394 nm respectively. The series of the characteristics of Europium (Eu^{3+}) ion emission centered at 485 and 518 respectively are ascribed mainly due to intra-4f transitions of $^7F_0 \rightarrow ^5D_2$ and $^7F_0 \rightarrow ^5D_1$ and for 486 and 536 nm are $^7F_0 \rightarrow ^5D_2$ and $^7F_1 \rightarrow ^5D_1$ respectively. In essence, visible emission could be attributed due to the various kinds of intrinsic defects such as defect states, zinc interstitials, oxygen vacancies, and zinc vacancies (Novotny et al., 2021). More compactly, when the concentration of dopant agent increased from (x=0.00-0.09), Europium (Eu^{3+}) ion- doping had a significant impact on the intensity (depending on the sample concentration), peak position (peak shifts), and emission spectra of bands(Xin, 2018) (Pal & Manam, 2013).

4.4.Fourier Transform Infra-Red (FT-IR) Analysis

The FT-IR spectra of both undoped and Europium (Eu^{3+}) ion doped Zinc Oxide nanoparticles (ZnO-NPs) were recorded at room temperature in the range of 400 cm^{-1} -4000 cm^{-1} with the resolution of 4 cm^{-1} using the KBr pellets. As it is shown in Figure 4.11, the absorption peaks for Undoped Zinc Oxide nanoparticles (ZnO-NPs) were observed at 3412, 2922, 1381, 841, and 566 cm^{-1}. The broad spectrum band located at 3412 cm^{-1} for undoped Zinc Oxide nanoparticles (ZnO-NPs) is due to the O-H stretching vibration mode. This can further manifest that the undoped Zinc Oxide nanoparticles (ZnO-NPs) show the presence of water molecules. Additionally, the other possible spectrum band located at 2922 cm^{-1} is attributed to the attachment of symmetric and asymmetric C-H groups (Naik et al., 2020).

Moreover, the broad absorption band located around 1381cm^{-1} is attributed to symmetric and asymmetric C=O stretching vibration modes (Ghrib et al., 2021).

The band observed around 841cm^{-1} is ascribed to the C-H out-of-plane bending for Zinc oxide nanoparticles (ZnO-NPs). Furthermore, the band located at around 566 cm^{-1} is attributed to the vibration of Zinc oxide nanoparticles (ZnO-NPs) (Vijayaprasath et al., 2018).

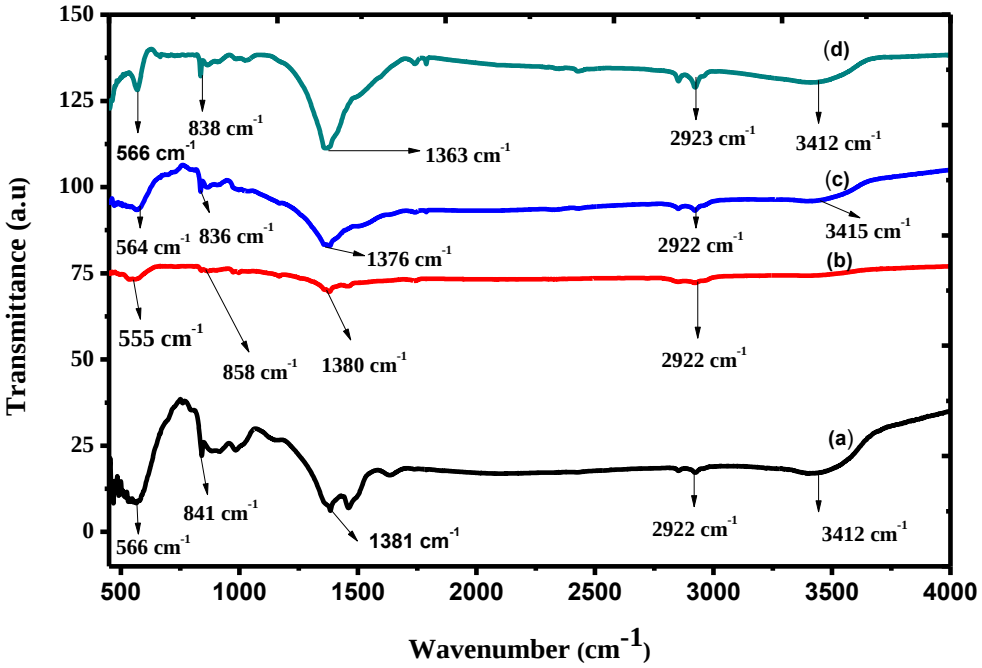

Figure 4.11: FT-IR spectra of synthesized of (a) Undoped and (b) $Zn_{0.97}Eu_{0.03}O$, (c) $Zn_{0.94}Eu_{0.06}O$, and (d) $Zn_{0.91}Eu_{0.09}O$ ZnO NPs.

The occurrence of Europium (Eu^{3+}) ions in the presence of Europium (Eu^{3+}) doped Zinc Oxide nanoparticles elucidated the presence of the peak at around 566 cm^{-1} in all the samples of Europium (Eu^{3+}) ion- doped Zinc Oxide nanoparticles. In the FT-IR spectrum band, there were no other additional bands were detected, this may be attributed to the substantiates of the synthesized product were almost pure without any significant impurity. With the further increase of doping concentration of Europium (Eu^{3+}) ion from (x=0.00-0.09) the absorption spectrum also observed as undoped Zinc Oxide nanoparticles (ZnO-NPs) leads to the vibration stretching mode of Zn-Eu-O which in turn asserts the successful substitution of Eu^{3+} ions into the Zn^{2+} sites. More interestingly, the existence of additional spectrum bands as the concentration increases reveals that Europium (Eu^{3+}) ion was successfully substituted into the ZnO host matrix. The absence of some peaks on Zinc Oxide nanoparticles (ZnO-NPs)

doped by Europium (Eu^{3+}) was might be due to the change in parameters and the bond properties of Zn perturbed by Eu. This means that the bonding properties of Eu are higher than that of the bonding properties of Zn.

4.5.Antibacterial Activity Studies

The antibacterial activity of (a) undoped ZnO NPs, (b) $Zn_{0.97}Eu_{0.03}O$ NPs, (c) $Zn_{0.94}Eu_{0.06}O$ NPs, and (d) $Zn_{0.91}Eu_{0.09}O$ NPs synthesized by co-precipitation method and annealed at a temperature of 500℃ suspensions of distinct concentrations towards the bacterial strains of Gram-positive bacteria ((*Escherichia coli, E. Coli*) and Gram-negative (*Staphylococcus aureus (S. aureus*)) bacteria were determined by the agar disc diffusion assay.

Figure 4.12: Antibacterial activity of Undoped, $Zn_{0.97}Eu_{0.03}O$, $Zn_{0.94}Eu_{0.06}O$, and $Zn_{0.91}Eu_{0.09}O$ ZnO NPs against *S. aureus*, *E. coli.*

The antibacterial activity of Undoped Zinc Oxide nanoparticles, Europium (Eu^{3+}) ion doped Zinc Oxide nanoparticles ($Zn_{0.97}Eu_{0.03}O$ NPs, $Zn_{0.94}Eu_{0.06}O$ NPs, and $Zn_{0.91}Eu_{0.09}O$ NPs) against the bacterial strains of Gram +ve and Gram –ve *S. aureus* and *E.coli* were tabulated and discussed in the table (4.4-4.7) respectively. The presence of an inhibition zone indicates that the mechanism of the biocidal action of ZnO nanoparticles involves disruption of the membrane with a high rate of generation of surface oxygen species and finally leads to the death of pathogens. Interestingly, the size of the inhibition zone was different according to the type of pathogens, synthesis method, and concentrations of ZnO nanoparticles (Gunalan et al., 2013). In

this work, the plausible three mechanisms, such as the release of Zn^{2+} and Eu^{3+} from Zinc Oxide (ZnO) complex into the bacteria containing the dissolution, generation of free radicals such as superoxide ion $O2^{-\bullet}$, hydroxyl ion $OH^{-\bullet}$, and Peroxide H_2O_2. Hydroxyl and superoxide ions fail to penetrate the cell membrane of bacteria due to their negative charge but peroxide ion easily penetrates the membrane and induces cell death (Abbaszadegan et al., 2015). Moreover, the electrostatic attraction of Zn^{+2} ions towards negatively charged membrane is also considered as one of the common ways of nanoparticle attachment to the cell surface. Zn^{+2} concentration in the bacterial cytoplasm is increased due to the local dissolution of attached Zinc Oxide nanoparticles (ZnO NPs) which leads to membrane leakage and loss of proton motive force.

Interestingly, in our study, the gram-negative bacteria for Undoped and Europium (Eu^{3+}) ion-doped Zinc Oxide nanoparticles ($Zn_{0.97}Eu_{0.03}O$ NPs, $Zn_{0.94}Eu_{0.06}O$ NPs, and $Zn_{0.91}Eu_{0.09}O$ NPs) has more susceptibility to nanoparticle-mediated toxicity as compared to gram-positive bacteria for Undoped and Europium (Eu^{3+}) ion doped Zinc Oxide nanoparticles ($Zn_{0.97}Eu_{0.03}O$ NPs, $Zn_{0.94}Eu_{0.06}O$ NPs, and $Zn_{0.91}Eu_{0.09}O$ NPs) since it has a thin layer of peptidoglycan as compared to gram-positive bacteria which exhibits less resistance on nanoparticle interaction with the cell membrane of gram-negative bacteria. Thus, cell wall thickness, structure, and composition play an important role in nanoparticle interaction with bacteria in the first place. In the inset of Figure (2.13-2.14) from the zone measurements, it could be explained that the Europium (Eu^{3+}) ion doped Zinc Oxide nanoparticles (ZnO-NPs) enhanced better antibacterial efficacy compared to Undoped to Zinc Oxide nanoparticles (ZnO-NPs). This work also reveals that the smaller particles exhibited higher bacterial activity due to the surface area to volume ratio of the materials.

Table 4.4: Zones of inhibition of Undoped Zinc Oxide nanoparticles (ZnO-NPs with different bacterial strains of a gram (+ve) and gram (-ve) bacteria with concentrations of 100 $\mu g/ml$, 150 $\mu g/ml$, and 200 $\mu g/ml$, and Ceftriaxone (+ve control).

Samples	Concentrations $\left(\mu g/ml\right)$	Zones of Inhibition (ZOI)
		Types of Pathogens (Gram +ve and Gram-ve)

		S. aureus	*E.coli*
Undoped ZnO-NPs	100	6.93±0.28	7.5±0.54
	150	7.2±0.25	7.6±0.50
	200	11.8±0.74	13±2.70
Ceftriaxone (+ve cont)	30	15.83±0.82	15.63±0.86

*Mean values of three replicates ± standard deviation

Table 4.5: Zones of inhibition of Europium doped Zinc Oxide nanoparticles ($Zn_{0.97}Eu_{0.03}O$ NPs) with different bacterial strains of a gram (+ve) and gram (-ve) bacteria with concentrations of 100 $\mu g/ml$, 150 $\mu g/ml$, 200 $\mu g/ml$, and Ceftriaxone (+ve control).

Samples	Concentrations $\left(\mu g/ml\right)$	Zones of Inhibition (ZOI)	
		Types of Pathogens (Gram +ve and Gram-ve)	
		S. aureus	*E.coli*
$Zn_{0.97}Eu_{0.03}O$ NPs	100	6.4±0.21	6.8±0.56
	150	6.6±0.13	7.1±0.99
	200	7.53±0.63	7.6±0.82
Ceftriaxone (+ve cont)	30	16.13±1.35	16.8±2.15

Table 4.6: Zones of inhibition of Europium doped Zinc Oxide nanoparticles ($Zn_{0.97}Eu_{0.03}O$ NPs) with different bacterial strains of a gram (+ve) and gram (-ve) bacteria with concentrations of 100 $\mu g/ml$, 150 $\mu g/ml$, 200 $\mu g/ml$, and Ceftriaxone (+ve control).

Samples	Concentrations $\left(\mu g/ml\right)$	Zones of Inhibition (ZOI)
		Types of Pathogens (Gram +ve and Gram-ve)

		S. aureus	*E.coli*
$Zn_{0.94}Eu_{0.06}O$ NPs	100	6.8±0.123	9.26±3.80
	150	6.86±0.330	7.43±1.820
	200	6.9±0.141	8.6±2.690
Ceftriaxone (+ve cont)	30	16.3±2.320	17.4±4.03

Table 4.7: Zones of inhibition of Europium doped Zinc Oxide nanoparticles ($Zn_{0.91}Eu_{0.09}O$ NPs) with different bacterial strains of gram (+ve) and gram (-ve) bacteria with concentrations of 100 $\mu g/ml$, 150 $\mu g/ml$, 200 $\mu g/ml$, and Ceftriaxone (+ve control).

Samples	Concentrations $\left(\mu g/ml\right)$	Zones of Inhibition (ZOI)	
		Types of Pathogens (Gram +ve and Gram-ve)	
		S. aureus	*E.coli*
$Zn_{0.91}Eu_{0.09}O$ NPs	100	6.8±0.250	7.3±0.760
	150	6.86±0.082	7.56±0.830
	200	7.2±0.130	7.6±0.170
Ceftriaxone (+ve cont)	30	17.56±1.990	18.36±0.822

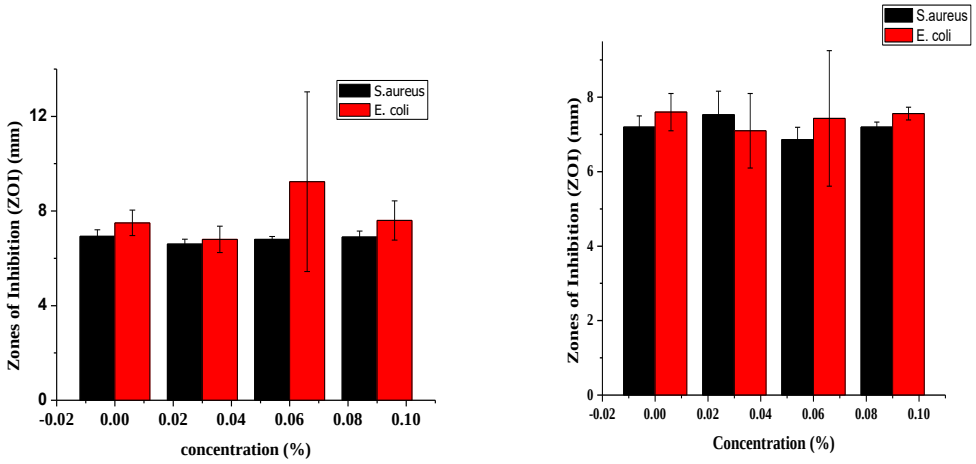

Figure 4.13: The size and Zones of inhibition formed around each disc for Undoped, $Zn_{0.97}Eu_{0.03}O$, $Zn_{0.94}Eu_{0.06}O$, and $Zn_{0.91}Eu_{0.09}O$ ZnO NPs with different bacterial strains of gram (+ve) and gram (-ve) bacteria with concentration of 100 $\mu g/ml$ and 150 $\mu g/ml$.

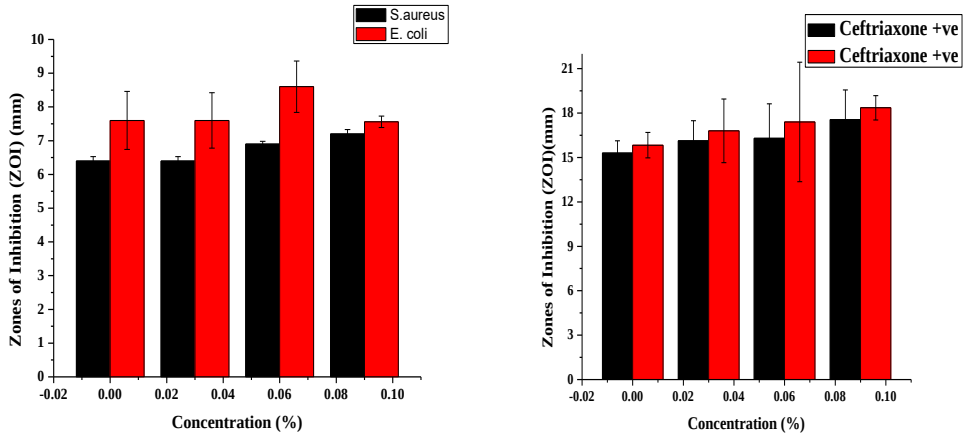

Figure 4.14: The size and Zones of inhibition formed around each disc for Undoped, $Zn_{0.97}Eu_{0.03}O$, $Zn_{0.94}Eu_{0.06}O$, and $Zn_{0.91}Eu_{0.09}O$ ZnO NPs with different bacterial strains of gram (+ve) and gram (-ve) bacteria with concentration of 200 $\mu g/ml$ and 30 $\mu g/ml$.

4.6.Photo-catalytic Activity

The photocatalytic activity of Undoped and Europium (Eu^{3+}) ion-doped Zinc Oxide nanoparticles (ZnO-NPs) were depicted in the inset of Figure 4.15 below towards the efficient degradation of methylene blue (MB) as an organic dye. It can be seen that

the UV-visible absorption spectra of degraded MB over the Undoped and Europium (Eu^{3+}) ion-doped Zinc Oxide nanoparticles (ZnO-NPs) under UV light illumination within 0–60 min over the wavelength range of 200–800 nm. It is noteworthy to see that the maximum absorption at λ_{peak} = 665 nm of MB dye is continuously decreased with the increase of exposure time from 0 to 60 min. From the given photo-degradation absorption spectra, the most intense absorption bands occurred at 665 nm, which was within the range of the absorption λ_{max} commonly reported from works of literature for MB degradation (Habib et al., 2021). In this study, the decrease in the relative intensities of absorption of Europium (Eu^{3+}) ion-doped ZnO is faster than that of pure Zinc Oxide nanoparticles (ZnO-NPs) which indicate that the Europium (Eu^{3+}) doping improves the effective performance degradation of dye under UV light illumination.

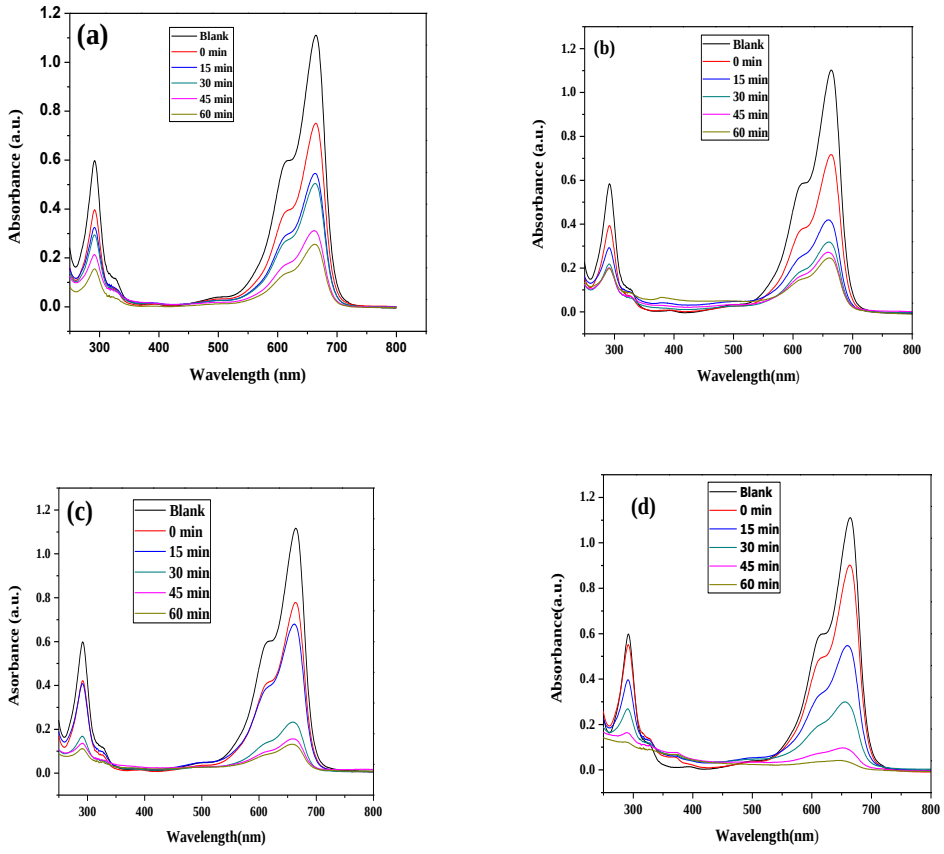

Figure 4.15: The absorption spectra for MB solutions containing (a) Undoped Undoped and (b) ($Zn_{0.97}Eu_{0.03}O$, (c) $Zn_{0.94}Eu_{0.06}O$ (d) $Zn_{0.91}Eu_{0.09}O$ ZnO NPs under UV light for different time intervals (0-60 min).

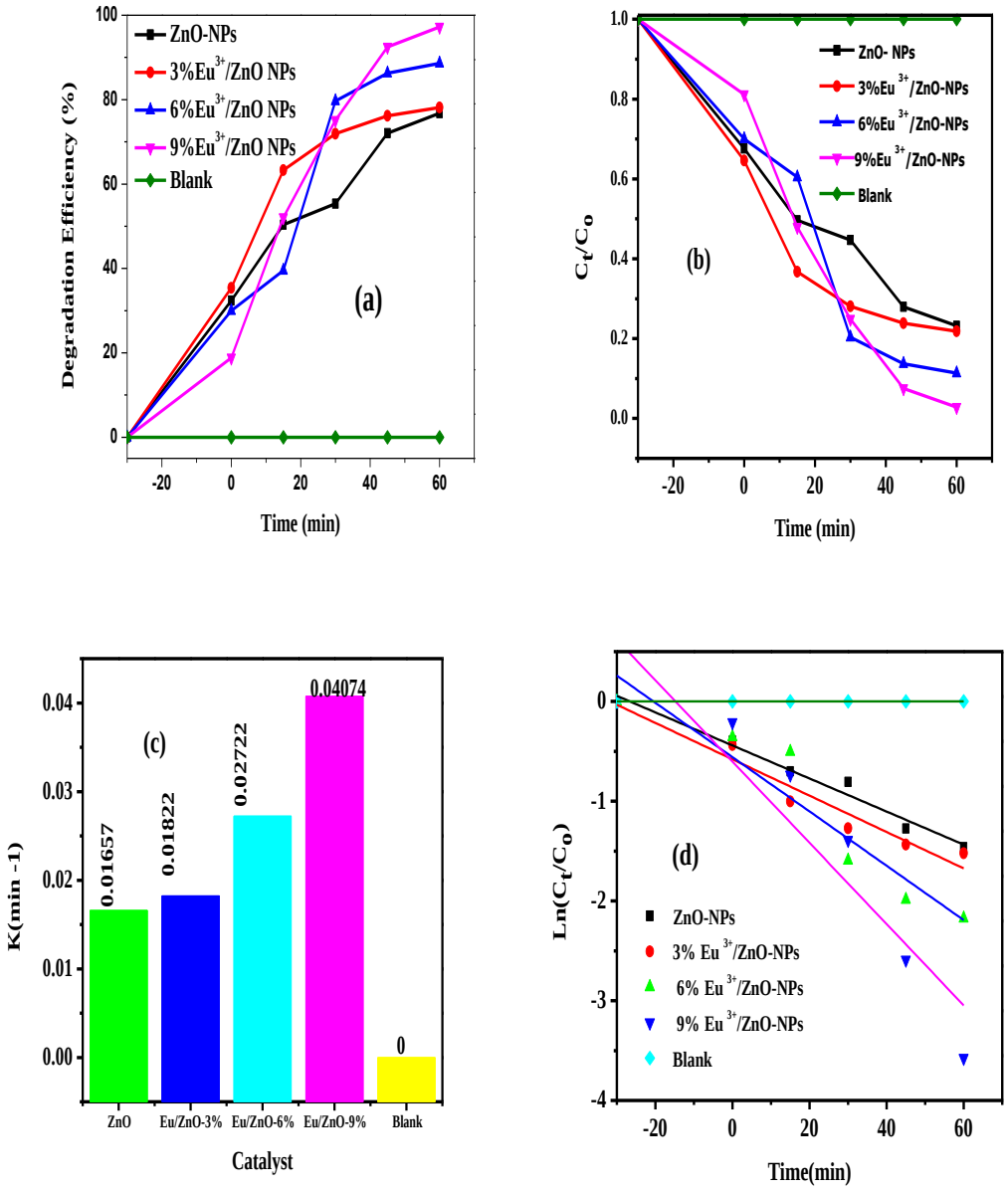

Figure 4.16: Photo-catalytic activity of (a) photocatalytic degradation analysis, (b) photocatalytic degradation kinetic curve study and, (c) photocatalytic degradation performance analysis respectively, and (d) photodegradation rate constants analysis for Undoped and $Zn_{0.97}Eu_{0.03}O$, $Zn_{0.94}Eu_{0.06}O$ $Zn_{0.91}Eu_{0.09}O$ ZnO NPs under UV light irradiation for different time intervals (0-60 min) respectively.

It is perceived that Undoped Zinc Oxide nanoparticles (ZnO-NPs) exhibit photo-degradation of MB solution of 76.8% which has been lower in the photo-degradation of the MB solution than Europium (Eu^{3+}) ion-doped Zinc Oxide nanoparticles (ZnO-NPs) samples. The photo-degradation efficiency of Europium (Eu^{3+}) ion-doped Zinc Oxide nanoparticles ($Zn_{0.97}Eu_{0.03}O$, $Zn_{0.94}Eu_{0.06}O$, and

$Zn_{0.91}Eu_{0.09}O$ ZnO NPs) were calculated to be 78.15%, 88.63%, and 97.2% respectively. Among the Europium (Eu^{3+}) ion-doped Zinc Oxide nanoparticles (ZnO-NPs) $Zn_{0.91}Eu_{0.09}O$ ZnO NPs have the highest photocatalytic activity which is higher than those of the Undoped ZnO and the other Europium (Eu^{3+}) ion-doped Zinc Oxide nanoparticles (ZnO-NPs) respectively. Figure 4.16(b) shows the absorption spectra of Undoped, and Europium (Eu^{3+}) ion-doped Zinc Oxide nanoparticles (ZnO-NPs) recorded at different irradiation times.

Photocatalytic activity for degradation of MB obeys the pseudo-first-order reaction kinetics with k as the rate constant and t as the UV irradiation time given by Eq (4.1) (Srinivasan, 2019).

$$C_t = C_o e^{-kt} \tag{4.1}$$

Where C_o and C_t are the concentrations of the MB at t = 0 and at the time of t, respectively.

The first-order kinetics referent to MB degradation has been carried out and the result is depicted in Fig. 4.16 (c). It shows the variation of ($\ln C_o/C_t$) as a function of UV exposure time for different Europium (Eu^{3+}) ion concentration photocatalysts, where Co and Co are the initial and final concentrations of MB. From this figure, it has been observed that all the four degradation graphs of MB follow the first pseudo order kinetics model depicted later. After discoloration of the dye, it has been monitored with respect to time and the reaction constant and the half-life time of the processes can be calculated under study. The low photocatalytic efficiency of (ZnO-NPs) is a result of the rapid recombination rate of the photo-induced carriers. For commercial applications, such as photo-catalytic degradation of contaminants the rate of recombination should be slow. In our study, it is observed that Europium (Eu^{3+}) ion-doped Zinc Oxide nanoparticles (ZnO-NPs) give better results than Undoped Zinc Oxide nanoparticles (ZnO). In Europium (Eu^{3+}) ion-doped ZnO, the (Eu^{3+}) ions create defect states which absorb the recombination pair by leaving the hydroxyl and amplify the photocatalytic efficiency. The synthesis method and ordering nature of the catalyst have also a high impact on this efficiency. A higher degree of crystallinity observed from the XRD result in Europium (Eu^{3+}) ion-doped samples may be one of the reasons responsible for this phenomenon. Generation of more and more hydroxyl ions takes place with an increase in UV irradiation time for the higher amount of

catalysts which provide a higher number of active sites on the surface. This makes chemical decomposition of more dye molecules containing complex organic structure

As discussed above, rare earth elements (REE), Europium (Eu^{3+}) are also involved in a charge transfer process with the host Zinc Oxide nanoparticles (ZnO) avoiding easy recombination of electron-hole pairs. The 4f-levels of these ions are the prime responsible factors for this process. From our study, it is predicted that the increased photocatalytic efficiency of Europium (Eu^{3+}) ion-doped Zinc Oxide nanoparticles (ZnO-NPs) can be greatly associated with the high surface adsorption ability and electron acceptor concentration of RE ions. Defect states like oxygen vacancy (V_O) unintentionally incorporated during the synthesis process can also act as electron scavenger to trap electrons and does not allow recombination of carrier and thus increased photo-catalytic performance.

5. CONCLUSIONS AND RECOMMENDATIONS

5.1. CONCLUSIONS

The Undoped and Europium (Eu^{3+}) ion-doped Zinc Oxide nanoparticles (ZnO-NPs) were synthesized via the co-precipitation method by using the Zinc Nitrate Hexahydrate as the starting materials, Europium Nitrate Pentahydrate as the dopant agent, Sodium Hydroxide as the precipitating agent. The synthesized samples for Undoped and Europium doped Zinc Oxide nanoparticles were then characterized by spectroscopic techniques such as X-ray Diffractometer (XRD), UV-Vis Spectroscopy, Photoluminescence (PL) Spectroscopy, and Fourier Transform Infra-Red (FT-IR) Spectroscopy. The XRD results revealed that the Undoped and Europium doped Zinc Oxide nanoparticles (ZnO-NPs) were hexagonal wurtzite crystal structures. No other peaks related to the samples are observed which are mainly attributed due to the successful incorporation of Europium (Eu^{3+}) ion into the host matrix. Furthermore, from the XRD studies the crystalline size of Undoped and Europium (Eu^{3+}) ion-doped Zinc Oxide nanoparticles (ZnO-NPs) were calculated to be 39.4 nm, 40.0 nm, 43.5 nm, and 45.0 nm respectively. The lattice parameters were also analyzed and stated in this work broadly.

From the UV-Vis Spectroscopy, the values of the energy bandgap were found to be 3.26 eV-3.28 eV. These results show that with further increase of the doping concentration of Eu^{3+} ions the bandgap value becomes wider which mainly resulted due to the Brustein-Moss Effect (BME) which is stated that the increase in the doping concentration amount perhaps the bandgap energy becomes wider. It has been also found that, from the Photoluminescence spectral analysis, the Undoped and Europium doped Zinc Oxide nanoparticles (ZnO-NPs) exhibited both near band edge emission and visible emission respectively. Likewise, as the doping concentration of Eu^{3+} increases, there are peak shifts for the higher doping concentrations. The FT-IR Spectroscopy revealed that the presence of the functional groups attached to the Undoped and Europium doped Zinc Oxide nanoparticles (ZnO-NPs) was ascertained which in turn is confirmed that, the Eu^{3+} substitutions of Eu^{3+} ion into the crystal lattice site of Zn^{2+}ions in the host matrix.

The antibacterial activity studies of Undoped and Europium doped Zinc Oxide nanoparticles (ZnO-NPs for the bacteria strains of Gram-positive (*S.aureus*) and Gram-negative (*E.coli*) were performed by using the agar disc diffusion methods. The result demonstrated that the Gram-negative bacteria exhibited more efficacy than Gram-positive bacteria. On the one hand, the higher doping concentration of Eu^{3+}possessed higher antibacterial activity compared to the lower concentration and undoped Zinc Oxide nanoparticles (ZnO-NPs).

The photocatalytic activity of Undoped and Europium (Eu^{3+}) ion- doped Zinc Oxide nanoparticles (ZnO-NPs) were investigated by Methylene Blue (MB) as organic dye solution and the result revealed that the degradation performance of Europium (Eu^{3+}) ion- doped Zinc Oxide nanoparticles (ZnO-NPs) were higher than that of Undoped Zinc Oxide nanoparticles (ZnO-NPs).

5.2.Recommendations

The doping method for the rare earth elements (REE) has been a hot research area in the future prospective. Further study regarding the doping method on rare earth elements (REE) is needed with ZnO NPs for multifunctional applications such as in the fields of the health system, nanomedicine, optoelectronic devices, and for producing light-emitting diodes.

In this work as the concentration of doping level increases its performance exhibit more efficiency for photodegradation of organic pollutants. So, the author can easily be forwarded that there exists an exceedingly increasing photodegradation of organic pollutants beyond the above results.

Research Fund Acknowledgment

This Research Project is funded by Adama Science and Technology University under the grant number ASTU/SM-R/260/21, Adama, Ethiopia.

BIBLIOGRAPHY

Abbaszadegan, A., Ghahramani, Y., Gholami, A., Hemmateenejad, B., Dorostkar, S., Nabavizadeh, M., & Sharghi, H. (2015). The effect of charge at the surface of silver nanoparticles on antimicrobial activity against gram-positive and gram-negative bacteria: A preliminary study. *Journal of Nanomaterials*, *1-10*. https://doi.org/10.1155/2015/720654

Ahmed, D., Osman, M., & Mustafa, M. A. (2015). Synthesis and Characterization of Zinc Oxide Nanoparticles using Zinc Acetate Dihydrate and Sodium Hydroxide. *1*(4), 248–251.

Amali, Z., Ramli, C., Asim, N., Isahak, W. N. R. W., Emdadi, Z., Ahmad-ludin, N., Yarmo, M. A., & Sopian, K. (2014). Photocatalytic Degradation of Methylene Blue under UV Light Irradiation on Prepared Carbonaceous TiO_2. *2014*(C), 13–15.

Azri, N., Aznan, K., & Johan, M. R. (2012). Quantum Size Effect in ZnO Nanoparticles via Mechanical Milling. *2012*, 1–5. https://doi.org/10.1155/2012/439010

Badreddine, K., Kazah, I., Rekaby, M., & Awad, R. (2018). Structural , Morphological , Optical , and Room Temperature Magnetic Characterization on Pure and Sm-Doped ZnO Nanoparticles. *2018*.

Belay, A., Getie, S., Chandra Reddy, A.R., & Belay, Z. (2017). Synthesis and Characterizations of Zinc Oxide Nanoparticles for Antibacterial Applications. Journal of Nanomedic Nanotechno S, https://doi.org/10.4172/2157-7439.S8-004

Bomila, R., Srinivasan, S., Venkatesan, A., Bharath, B., & Perinbam, K. (2018). Structural, optical and antibacterial activity studies of Ce-doped ZnO nanoparticles prepared by wet-chemical method. *Materials Research Innovations*, *22*(7), 379–386. https://doi.org/10.1080/14328917.2017.1324379

Bunaciu, A. A., & Aboul-enein, H. Y. (2015). X-Ray Diffraction : Instrumentation and Applications Critical Reviews in Analytical Chemistry X-Ray Diffraction :

Instrumentation and Applications.. https://doi.org/10.1080/10408347.2014.949616

Choi, B., Lee, H., Jin, S., & Chun, S. (2007). Characterization of the optical properties of silver nanoparticle films. Nanotechnology, 18(7), 1-5. https://doi.org/10.1088/0957-4484/18/7/075706.

Choudhary, I. (2020). Effect of excitation wavelength and europium doping on the optical properties of nanoscale zinc oxide. *Journal of Materials Science: Materials in Electronics*, *31*(22), 20033–20042. https://doi.org/10.1007/s10854-020-04525-x

Daksh, D., & Agrawal, Y. K. (2016). Rare Earth-Doped Zinc Oxide Nanostructures : A Review. *5*(1), 1–27. https://doi.org/10.1166/rnn.2016.1071

Dash, D., Panda, N. R., & Sahu, D. (2019). Applied Surface Science Photoluminescence and photocatalytic properties of europium doped ZnO nanoparticles. *Applied Surface Science*, *494*, 666–674. https://doi.org/10.1016/j.apsusc.2019.07.089

Devi, P. G., & Velu, A. S. (2016a). Structural , optical and photoluminescence properties of copper and iron doped nanoparticles prepared by co-precipitation method. *Journal of Materials Science: Materials in Electronics*, *27*(10), 10833–10840. https://doi.org/10.1007/s10854-016-5190-1

Devi, P. G., & Velu, A. S. (2016b). Synthesis, structural and optical properties of pure ZnO and Co doped ZnO nanoparticles prepared by the co-precipitation method. *Journal of Theoretical and Applied Physics*, *10*(3), 233–240. https://doi.org/10.1007/s40094-016-0221-0

Dumrongrojthanath, P., & Phuruangrat, A. (2021). Photocatalysis of Cd-doped ZnO synthesized with precipitation method. *Rare Metals*, *40*(3), 537–546. https://doi.org/10.1007/s12598-019-01283-6

Emami-karvani, Z., & Chehrazi, P. (2011). Antibacterial activity of ZnO nanoparticle on gram- positive and gram-negative bacteria. *5*(12), 1368–1373. https://doi.org/10.5897/AJMR10.159

Gadalla, A. A., Abood, I., & Elokr, M. M. (2018). Structural , Optical and Magnetic

Properties of Ni-Doped ZnO Synthesized by Co-Precipitation Method. *February*. https://doi.org/10.15436/2377-1372.17.1374

Ghrib, T., Massoudi, I., Otaibi, A. L. Al, Al, A., Aya, M., Eman, K., & Hashem, A. (2021). Effects of Terbium Doping on Structural , Optical and Photocatalytic Properties of ZnO Nanopowder Prepared by Solid - State Reaction. *Journal of Inorganic and Organometallic Polymers and Materials*, *31*(1), 239–250. https://doi.org/10.1007/s10904-020-01761-w

Guan, R., Li, J., Zhang, J., Zhao, Z., Wang, D., & Zhai, H.,& Sun, D. (2019). Photocatalytic Performance and Mechanistic Research of ZnO / g - C 3 N 4 on Degradation of Methyl Orange. ACS Omega, 4(24), 20742-20747. https://doi.org/10.1021/acsomega.9b03129

Gunalan, S., Sivaraj, R., & Rajendran, V. (2013). Progress in Natural Science : Materials International Green synthesized ZnO nanoparticles against bacterial and fungal pathogens. *Progress in Natural Science: Materials International*, *22*(6), 693–700. https://doi.org/10.1016/j.pnsc.2012.11.015

Habib, I. Y., Zain, N. M., Lim, C. M., Usman, A., Kumara, N. T. R. N., & Mahadi, A. H. (2021). Effect of Doping Rare-Earth Element on the Structural, Morphological, Optical and Photocatalytic Properties of ZnO Nanoparticles in the Degradation of Methylene Blue Dye. *IOP Conference Series: Materials Science and Engineering*, *1127*(1), 012004. https://doi.org/10.1088/1757-899x/1127/1/012004

Hahn, Y. (2011). Zinc oxide nanostructures and their applications. *28*(9), 1797–1813. https://doi.org/10.1007/s11814-011-0213-3

Hoseinzadeh, E., Makhdoumi, P., Taha, P., Hossini, H., Stelling, J., Kamal, M. A., & Ashraf, G. (2017). A Review on Nano-Antimicrobials : Metal Nanoparticles , Methods , and Mechanisms. Current drug metabolisms, 18(2), 120-128. https://doi.org/10.2174/1389200217666161201111

Jeetendra, S., Nagabhushana, H., Mrudula, K., Naveen, C. S., Raghu, P., & Mahesh, H. M. (2014). Concentration Dependent Optical and Structural Properties of Mo doped ZnTe Thin Films Prepared by e-beam Evaporation Method. *9*, 2944–2954.

Karakız, M., Altunbas, M., Bacaksiz, E., Parlak, M., Tomakin, M., & Ozc, A. (2008). The effects of zinc nitrate , zinc acetate and zinc chloride precursors on investigation of structural and optical properties of ZnO thin films. *466*, 447–450. https://doi.org/10.1016/j.jallcom.2007.11.061

Karthick, C. S. N. A. R. (2018). Investigation on structural , morphology and photoluminescence properties of lanthanum doped zinc oxide nanostructure for optical application by co-precipitation method. *Journal of Materials Science: Materials in Electronics*, *29*(13), 11553–11558. https://doi.org/10.1007/s10854-018-9251-5

Karthikeyan, C., Arun, L., Hameed, A. S. H., Gopinath, K., Umaralikahan, L., Vijayaprasath, G., & Malathi, P. (2019). Structural, optical, thermal and magnetic properties of nickel calcium and nickel iron co-doped ZnO nanoparticles. *Journal of Materials Science: Materials in Electronics*, *30*(9), 8097–8104. https://doi.org/10.1007/s10854-019-01160-z

Kaur, M., Kaur, P., Kaur, G., Dev, K., Negi, P., & Sharma, R. (2018). Structural, morphological and optical properties of Eu-N co-doped zinc oxide nanoparticles synthesized using co-precipitation technique. *Vacuum*, *155*(May), 689–695. https://doi.org/10.1016/j.vacuum.2018.06.046

Koao, L. F., Dejene, B. F., Swart, H. C., Motloung, S. V, & Motaung, T. E. (2016). Characterization of annealed Eu^{3+} -doped ZnO fl ower-like morphology synthesized by chemical bath deposition method. *Optical Materials*, *60*, 294–304. https://doi.org/10.1016/j.optmat.2016.07.042

Korake, P. V, Kadam, A. N., & Garadkar, K. M. (2014). Photocatalytic activity of Eu^{3+} -doped ZnO nanorods synthesized via microwave assisted technique. *Journal of Rare Earths*, *32*(4), 306–313. https://doi.org/10.1016/S1002-0721(14)60072-7

Kumar, P., Singh, B. K., Pal, B. N., & Pandey, P. C. (2016). Correlation between structural , optical and magnetic properties of Mn-doped ZnO. *Applied Physics A*, *122*(8), 1–12. https://doi.org/10.1007/s00339-016-0265-7

Labhane, P. K., Sonawane, G. H., & Sonawane, S. H. (2018). Influence of rare-earth metal on the zinc oxide nanostructures : application in the photocatalytic degradation of methylene blue and p-nitro phenol. 360–371.

Lu, J. G., Fan, Z., & Lu, J. G. (2005). Zinc Oxide Nanostructures : Synthesis and Properties Zinc Oxide Nanostructures : Synthesis and Properties. https://doi.org/10.1166/jnn.2005.182

Ma, X., & Wang, Z. (2012). Materials Science in Semiconductor Processing The optical properties of rare earth Gd doped ZnO nanocrystals. *Materials Science in Semiconductor Processing*, *15*(3), 227–231. https://doi.org/10.1016/j.mssp.2011.05.013

Moballegh, A. (2007). ZnO nanoparticles obtained by mechanochemical technique and the optical properties. *Surface Science 601(13)*, 2850–2854. https://doi.org/10.1016/j.susc.2006.12.012

Naik, E. I., Naik, H. S. B., Suresh, R. V. I. K., & Prabhakara, G. M. C. (2020). Bright red luminescence emission of macroporous honeycomb - like Eu^{3+} ion - doped ZnO nanoparticles developed by gel - combustion technique. *SN Applied Sciences*, *2*(5), 1–13. https://doi.org/10.1007/s42452-020-2639-x

Nano-tio, P. A. (2015). Evaluation on the Photocatalytic Degradation Activity of Reactive Blue 4 using Evaluation on the Photocatalytic Degradation Activity of Reactive. https://doi.org/10.17576/jsm-2015-4407-13

Novotny, M., Fitl, P., Remsa, J., Kiisk, V., Luka, F., Fekete, L., Volfova, L., Kodu, M., Jaaniso, R., Hrus, P., Vrn, M., Lanc, J., & Vondra, M. (2021). Effect of pulsed laser annealing on optical and structural properties of ZnO : Eu thin film. Journal of *Materials Science,* 59(19)11414–11425. https://doi.org/10.1007/s10853-021-06030-w

Ntwaeaborwa, O. M., Mofokeng, S. J., Kumar, V., & Kroon, R. E. (2017). Structural, optical and photoluminescence properties of Eu^{3+} doped ZnO nanoparticles. *Spectrochimica Acta - Part A: Molecular and Biomolecular Spectroscopy*, *182*, 42–49. https://doi.org/10.1016/j.saa.2017.03.067

Pal, P. P., & Manam, J. (2013). Structural and photoluminescence studies of Eu^{3+} doped zinc oxide nanorods prepared by precipitation method. *Journal of Rare Earths*, *31*(1), 37–43. https://doi.org/10.1016/S1002-0721(12)60231-2

Parihar, V., Raja, M., & Paulose, R. (2018). A Brief Review Of Structural , Electrical

And Electrochemical Properties Of Zinc Oxide Nanoparticles.

Phuruangrat, A., Dumrongrojthanath, P., Yayapao, O., Arin, J., Thongtem, S., & Thongtem, T. (2016). Photocatalytic activity of La-doped ZnO nanostructure materials synthesized by sonochemical method. *Rare Metals*, *35*(5), 390–395. https://doi.org/10.1007/s12598-015-0508-3

Phuruangrat, A., Yayapao, O., Thongtem, T., & Thongtem, S. (2014). Synthesis and Characterization of Europium-Doped Zinc Oxide Photocatalyst. Journal of Nanomaterials, *2014*.

Pradeev, K., Sadaiyandi, K., Kennedy, A., Sagadevan, S., Chowdhury, Z. Z., Rafie, M., Johan, B., Aziz, F. A., Rafique, R. F., Selvi, R. T., & Rathina, R. (2018). Influence of Mg Doping on ZnO Nanoparticles for Enhanced Photocatalytic Evaluation and Antibacterial Analysis.

Preethi, S., Anitha, A., & Arulmozhi, M. (2016). A Comparative Analysis of the Properties of Zinc Oxide (ZnO) Nanoparticles Synthesized by Hydrothermal and Sol-Gel Methods. *Indian J Sci Techno*, 1–6. https://doi.org/10.17485/ijst/2016/v9i40/92696

Raj, K. P., Kennedy, K. S. A., & Sagadevan, S. (2017). Photocatalytic and antibacterial studies of indium-doped ZnO nanoparticles synthesized by co-precipitation technique. *Journal of Materials Science: Materials in Electronics*, *28*(24), 19025–19037. https://doi.org/10.1007/s10854-017-7857-7

Raj, K. P., Sadaiyandi, K., Kennedy, A., & Thamizselvi, R. (2016). Structural , optical , photoluminescence and photocatalytic assessment of Sr-doped ZnO nanoparticles. *Materials Chemistry and Physics*, *183*, 24–36. https://doi.org/10.1016/j.matchemphys.2016.07.068

Ramírez, A. E., Muñoz, M. M., López, L. L., Ibarra, J. E. R., Coaquira, J. A. H., Heinrichs, B., & Páez, C. A. (2021). Significantly enhancement of sunlight photocatalytic performance of ZnO by doping with transition metal oxides. *Scientific Reports*, *0123456789*, 1–9. https://doi.org/10.1038/s41598-020-78568-9

Rl, M., Kv, U., & Naik, D. (2019). Synthesis and characterization of ZnO

nanoparticles : A review. *8*(3), 1095–1101.

Sa-nguanprang, S., Phuruangrat, A., Thongtem, T., & Thongtem, S. (2019). Synthesis, Analysis, and Photocatalysis of Mg-Doped ZnO Nanoparticles. *Russian Journal of Inorganic Chemistry*, *64*(14), 1841–1848. https://doi.org/10.1134/S0036023619140158

Salahuddin, N. A., El-kemary, M., & Ibrahim, E. M. (2015). Synthesis and Characterization of ZnO Nanoparticles via Precipitation Method : Effect of Annealing Temperature on Particle Size. *5*(4), 82–88. https://doi.org/10.5923/j.nn.20150504.02

Sharma, D. K., Kumar, K., & Vipin, S. (2016). Effect of Ce doping on the structural , optical and magnetic properties of ZnO nanoparticles. *Journal of Materials Science: Materials in Electronics*, *27*(10), 10330–10335. https://doi.org/10.1007/s10854-016-5117-x

Sharma, R. K., & Ghose, R. (2015). Synthesis of zinc oxide nanoparticles by homogeneous precipitation method and its application in antifungal activity against Candida albicans. *Ceramics International*, *41*(1), 967–975. https://doi.org/10.1016/j.ceramint.2014.09.016

Siddiqi, K. S., Rahman, A., & Husen, A. (2018). Properties of Zinc Oxide Nanoparticles and Their Activity Against Microbes.

Sirelkhatim, A., Mahmud, S., & Seeni, A. (2015). Review on Zinc Oxide Nanoparticles : Antibacterial Activity and Toxicity Mechanism. *Nano-Micro Letters*, *7*, 219–242. https://doi.org/10.1007/s40820-015-0040-x

Srinivasan, R. B. S. S. S. (2019). Synthesis , characterization and comparative studies of dual doped ZnO nanoparticles for photocatalytic applications. *Journal of Materials Science: Materials in Electronics*, *30*(1), 582–592. https://doi.org/10.1007/s10854-018-0324-2

Stefaniuk, I., Cieniek, B., Rogalska, I., Virt, I. S., & Kosciak, A. (2018). Magnetic properties of ZnO:Co layers obtained by pulsed laser deposition method. *Materials Science- Poland*, *36*(3), 439–444. https://doi.org/10.1515/msp-2017-0114

Tafreshi, M. M. M. J. (2020). Gadolinium doping affecting on structural , magnetic and dielectric properties of ZnO nanoparticles. *Applied Physics A*, *126*(4), 1–8. https://doi.org/10.1007/s00339-020-3456-1

Universit, T., & Ilmenau, Y. F. (2017). Structural Parameters (Size , Defect and Doping) of ZnO Nanostructures and Relations with their Optical and Electrical Properties Dissertation.

Upadhyaya, H., Shome, S., Sarma, R., & Tewari, S. (2018). Green Synthesis , Characterization and Antibacterial Activity of ZnO Nanoparticles. 1279–1291. https://doi.org/10.4236/ajps.2018.96094

Vijayaprasath, G., Murugan, R., Asaithambi, S., Babu, G. A., Sakthivel, P., Mahalingam, T., Hayakawa, Y., & Ravi, G. (2016). Structural characterization and magnetic properties of Co co-doped Ni/ZnO nanoparticles. *Applied Physics A: Materials Science and Processing*, *122*(2), 1–11.

Vijayaprasath, G., Murugan, R., Palanisamy, S., Prabhu, N. M., Mahalingam, T., Hayakawa, Y., & Ravi, G. (2015). Structural, optical and antibacterial activity studies of neodymium doped ZnO nanoparticles. *Journal of Materials Science: Materials in Electronics*, *26*(10), 7564–7576.

Vijayaprasath, G., Soundarrajan, P., & Ravi, G. (2018). The point defects induced ferromagnetism in ZnO semiconductor by terbium doping via co-precipitation method. *Journal of Materials Science: Materials in Electronics*, *29*(14), 11892–11900. https://doi.org/10.1007/s10854-018-9290-y

Wang, Z. L. (2004). Zinc oxide nanostructures : growth , properties and applications applications. https://doi.org/10.1088/0953-8984/16/25/R01

Xin, M. (2018). Effect of Eu doping on the structure, morphology and luminescence properties of ZnO submicron rod for white LED applications. *Journal of Theoretical and Applied Physics*, *12*(3), 177–182.

Zhang, N., Chen, D., Niu, F., Wang, S., Qin, L., & Huang, Y. (2016). Enhanced visible light photocatalytic activity of Gd-doped $BiFeO_3$ nanoparticles and mechanism insight. *Scientific Reports*, 1–11. https://doi.org/10.1038/srep26467